UNIVERSITY OF NAIROBI

"SLOPE STABILITY ANALYSIS USING TECTOSTRUCTURAL AND GEOTECHNICAL PARAMETERS: A CASE STUDY OF TSHONDO AREA, SOUTH-KIVU REGION (DRC)"

BY

AGANZE BACIYUNJUZE GLOIRE

Reg: I56/89311/2016

A DISSERTATION SUBMITTED TO THE DEPARTMENT OF GEOLOGY IN PARTIAL FULFILLMENT OF THE REQUIREMENTS FOR THE DEGREE OF MASTERS OF SCIENCE IN GEOLOGY (ENGINEERING GEOLOGY) OF THE UNIVERSITY OF NAIROBI.

OCTOBER 2018

DECLARATION

I declare that this thesis is my original work and has not been submitted elsewhere for examination, award of degree or publication. Where other people's work or my own work has been used, this has been properly acknowledged and referenced in accordance with the University of Nairobi's requirements.

Signed……………………………………… Date………………………………

AGANZE BACIYUNJUZE Gloire.
I56/89311/2016
Department of Geology
School of Physical Sciences
University of Nairobi

This thesis has been submitted for examination with our approval as supervisors:

	Signature	Date

Dr. Aaron Kutukhulu Waswa   ………………   …………….
aaronwaswa@gmail.com
Department of Geology
University of Nairobi
PO Box 30197-00100
Nairobi, KENYA

Dr. Lydia Olaka Atieno   …………….   ………………
lydiaolaka@uonbi.ac.ke
Department of Geology
University of Nairobi

This form must be completed and signed for all works submitted to the University for Examination.

Name of Student: AGANZE BACIYUNJUZE Gloire

Registration Number: I56/89311/2016

College: BIOLOGICAL AND PHYSICAL SCIENCES

Faculty/School/Institute: SCHOOL OF PHYSICAL SCIENCES

Department: GEOLOGY

Course Name: Msc. in Geology

Title of the work: **SLOPE STABILITY ANALYSIS IN THE NEOPROTEROZOIC TERRAINS USING TECTOSTRUCTURAL AND GEOTECHNICAL PARAMETERS: A CASE STUDY OF TSHONDO AREA, SOUTH-KIVU (DRC)**

DECLARATION

1. I understand what Plagiarism is and I am aware of the University's policy in this regard

2. I declare that this _____ (Thesis, dissertation, project, essay, assignment, paper, report, etc.) is my original work and has not been submitted elsewhere for examination, award of a degree. Where other people's work, or my own work has been used, this has properly been acknowledged and referenced in accordance with the University of Nairobi's requirements.

3. I have not sought or used the services of any professional agencies to produce this work

4. I have not allowed, and shall not allow anyone to copy my work with the intention of passing it off as his/her own work

5. I understand that any false claim in respect of this work shall result in disciplinary action, in accordance with University Plagiarism Policy.

Signature _____

Date _____

DEDICATION

To my dear Father BASHIMBE BACIYUNJUZE VINCENT and my beloved Mother
ANASTASIE M'CIZUNGU
To my brothers and sisters, my friends and comrades

To the person with whom my soul will be bound by fate and all the beings that will
result from this union for the rest of our lives

To all the victims of landslides due to the instability of slopes at Tshondo,

I dedicate this work.

ACKNOWLEDGEMENTS

ABSTRACT

The study area is located in the Democratic Republic of the Congo, along the western branch of the East African Rift. The problem within this highly strained zone, is the lack of knowledge on slope stability and the diversity of interpretations emanating from several researchers on the geology and the tectonic evolution of Tshondo area. The study aims at broadly assessing the stability of slopes using tectonic, structural and geotechnical input parameters. In order to achieve this objective, a multidisciplinary approach has been adopted in this research.

The structural survey has provided a comprehensive understanding of the tectonic evolution of Tshondo area and how different fractures influence on slope stability. Two phases of deformation were acknowledged by the PT and the Right Dieder methods: The extensional and the compressional deformation phases, highlighted by fractures generally trending NW-SE. The stress tensors responsible for these phases are made of principal axes defined such as $\sigma_1 \geq \sigma_2 \geq \sigma_3$ and $\sigma_3 \geq \sigma_1 \geq \sigma_2$. The corresponding stress ratios were, respectively R= 0.46 and 2.5. On a Mohr diagram, the failure analysis provided some slip tendency values (T's) ranging from 1 to 0. The fault planes were above the critical stress (0.8 < T's < 1), the joints, tensile and conjugate fractures were close to the critical stress (0.4 < T's < 0.8), and the bedding planes were far below the main frictional line (0 < T's < 0.4).

The geotechnical field and laboratory investigations have revealed the presence of cohesionless soils on the upper horizons of the slope profiles. The underlying rocks presented poor strengths. Their undrained cohesion (Cu) values were 20.5 Kpa for completely weathered black shale, 19.5 Kpa for moderately weathered conglomerate, 32 Kpa and 27 Kpa for highly weathered sandstone and pelite. The thin section microscopy has revealed the presence of high proportions of clay minerals and oxides in most of these rock samples. The computation of the safety factors provided some values < 1: Respectively, 0.74 < FoS < 1 for slope 1, and 0.48 < FoS < 1 for slope 2. After applying the seismic coefficient of 0.21 in the pseudostatic analysis, these safety factors further reduced to 0.55 < FoS < 1 for slope 1, and 0.36 < FoS < 1 for slope 2.

Key-words*: Tshondo, strained zone, paleostress, slip tendency, tectonic evolution, pseudostatic analysis.*

TABLE OF CONTENTS

LIST OF TABLES

LIST OF FIGURES

LIST OF APPENDICES

LIST OF ACRONYMS, SYMBOLS AND INITIALS

ASTM: American society for Testing and Materials

BS: British Standards

CIA: Chemical Index of Alteration

C_C: Coefficient of curvature

C_U: Coefficient of Uniformity

CU: Undrained Cohesion

C.W: Completely weathered

DEM: Digital elevation model

D1:   Deformation 1

D2:   Deformation 2

FoS: Factor of Safety

IRSAC: Institut pour la Recherche Scientifique en Afrique Centrale

ISRM: International society of rock mechanics).

DRC: The Democratic Republic of the Congo

H.W: Highly weathered

GIS: Geographical Information system

Kg: Kilogram

Kpa: Kilopascal

M.D: Moderately weathered

PT: Kinematic axes (P: pressure axis, B: T: tension axis)

Su: Undrained Shear Strength

UCS: Unconfined (Uniaxial) Compressive strength

T's: Normalized slip tendency

WIP: Weathering Index.

CHAPTER 1 : INTRODUCTION

1.1 BACKGROUND INFORMATION

The different aspects of the earth's surface today, evolve in an unprecedented way. The latter is altered under human actions and activities and more generally under the action of other factors which are undoubtedly the most constraining, associated with the succession of geological events by natural law. The word "slope" may be defined as an elevated land with surfaces that are at an angle. Slope stability, on the other hand, is the study of the mechanical balance of soil or rock masses.

The analysis of slope stability at Tshondo is a very complex study. Its understanding, especially in such a mountainous area, made of active deformations, requires a meticulous analysis of both geological and non-geological parameters. It is actually a multidisciplinary study, involving a good number of branches of geology. However, our study only focused on the structural interpretation of discontinuities encountered along the slopes as well as the analysis of the physico-mechanical properties of soils and rocks.

The actual morphology of Tshondo shows a landscape history of a highly unstable area, which by its geographical position has been intensely strained during the Pan-African period by the submeridian tectonics. Relying on Cahen (1954) and Ilunga (1989) works, these stresses, the related deformations as well as the geological structures, are nowadays being reported as precursors of several slope failures within the South-Kivu region. These failures are further triggered by the fluctuation in factors such as soil and rock types, material properties, weathering intensity, human activities, climate, vegetation, etc.

The auriferous mineralization is petrographically hosted in incompetent rocks, which are layers of weathered to slightly consolidated black shales, but also highly weathered pelites similar to sandstones, often micaceous, isolated in a clay matrix rich in biotite and chlorite (Walemba, 2001; Villeneuve, 1977). This lithology can also act as a plane of weakness and can, therefore, be a limiting factor for slope stability. From what precedes and obviously to a problem as serious as this, something has to be done. Human lives need to be preserved and the environment needs to be protected. Overlooking this issue may result in the destruction of Tshondo's environment and furthermore its extinction.

1.2 STATEMENT OF THE PROBLEM

Since the earliest times, the understanding of geological parameters for the apprehension of the behavior of soil masses and sloping rocks in areas made of active deformations, has been a process impeded by a range of uncertainties and a diversity of interpretations for more than one engineer. During the past 15 years, the increase in the number of artisanal miners, combined with the environmental impacts inherited from long years of mining without an adequate grading of slopes, has not only worsened the state of the environment at Tshondo, but also led to the loss of human lives. Dreadful situations have been witnessed in 2016. About 10 people have lost their lives in Tshondo's mining quarry. It is in regard of these problems that a stability study needs to be undertaken.

1.3 THE STUDY AREA

1.3.1 Location and Description

Tshono area is located in the Democratic Republic of the Congo, approximately 95 km southwest of Bukavu city (Figure 1.1Aa). This zone of sloping hills covers an area of 20 km^2 and is bounded by longitudes 28.60°E and 28.65°E, and the latitudes -2.87°S and -2.89°S (Figure1.2b). The area is subjected to an artisanal and small-scale mining exploitation. About 100 miners operate in the quarry
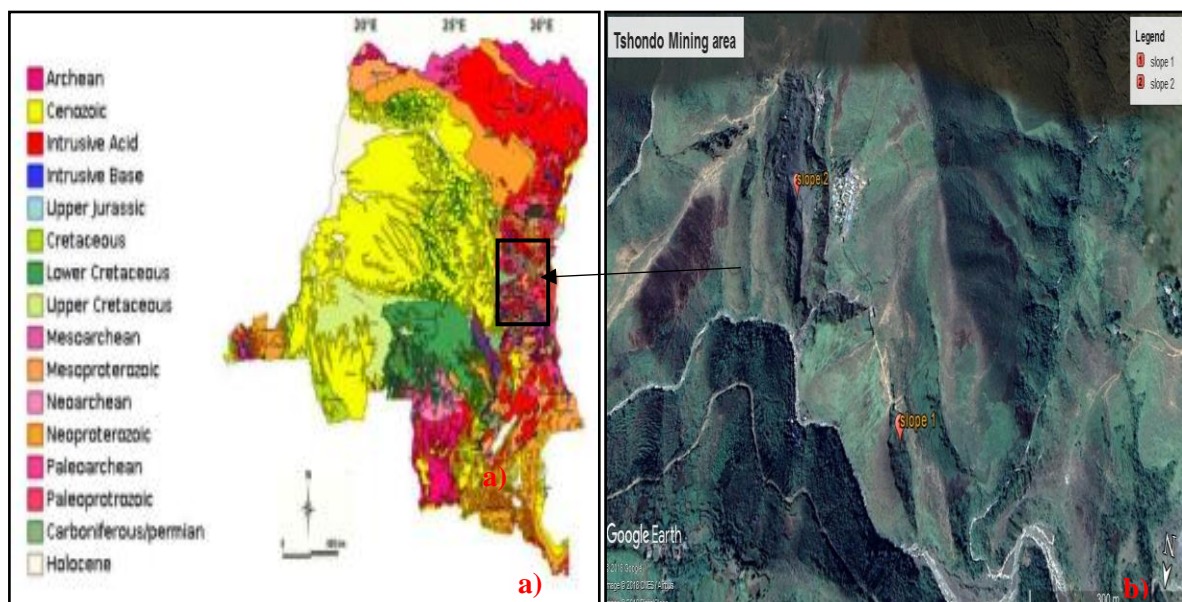
Figure 1.1: Democratic Republic of the Congo (a), Panoramic view of the analyzed slopes (c).

1.3.2 Climate and vegetation

The climate at Tshondo is tropical. The weather station in Bujumbura, used to estimate the climate in the area, shows that September is the hottest month of the year with temperatures averaging 25°C (Figure 1.2b). The average rainfall of 14.9 mm makes June the driest month. In February, the rainfall is significant with an average of 79 mm (Figure 1.2a). The heat record throughout time was 39°C on May 20th, 1978 and the cold record was 2°C on February 11st, 1993.
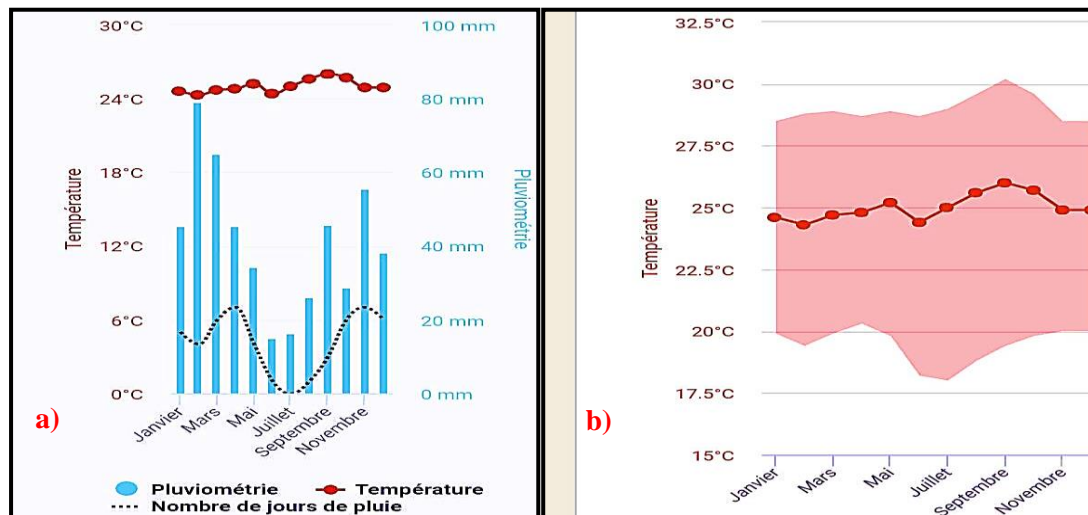
Figure 1.2 : Graph of maximum rainfall (a) and average temperature (b) at Tshondo.

Tshondo area is favorable for any kind of cultivation due to its tropical climate. It rains mainly between mid-September and early June. Food crops such as cassava, beans, bananas, sweet potatoes, maize, etc. are cultivated. There are also enormous possibilities for industrial crops such as tea, coffee and palm oil. 50% of Tshondo area is occupied by the forest which is mostly made of cypresses and eucalyptus. The vegetation is grassy luxuriant - evergreen, giving a meadow that confers to the zone a vocation of breeding (Erick *et al.,* 2010). Towards the south and the south-west, on the slope of the right bank of Mushenyi river, a natural forest is still present. Forest formations grow on mountainsides, hills and plateaus with altitudes between 900 m and 3475 m. The parts above 3,000 m were formerly occupied by some bamboo plantations, but a huge part of them have been destroyed. Nowadays, this area is mainly controlled by Pteridium aquilinum formations (Wilson *et al*., 1990).

1.3.3 Current land use and land resources

Tshondo, according to the works of Walemba KMA (2001) and Villeneuve (2004), is made of a panoply of mineralization of which the most important are auriferous and would derive from the albitite originated from the Kasika granite. Lands are used rationally, among other things,

for single-family dwellings, public buildings such as schools (the Kakwende Institute is the most famous in the area), churches, and residence. Constructions are made of straws in some places, but mostly in durable material, given the fact that local residents are engaged in the manufacturing of building bricks. Both mining and agricultural occupy prominent positions, and constitute the backbones to Tshondo's economy.

Figure 1.3 : Extraction of auriferous ores by artisanal miners at Tshondo.

1.3.4   Physiography and Drainage

On the regional scale, the greater part of the Itombwe Mountain lies above 1,500 m, the highest point being made up of highlands above 2,000 m. The terrain rises from 900 m to Itula (South-West), 1,100 m to Kamituga (West), and to the highest peaks in the north and east of Tanganyika lake (773 m above sea level). These summits regularly reach or exceed 3,000 m; the highest being Mount Mohi (3,475 m). The relief of Tshondo is more or less accentuated and dominated by a hilly topography. The area is made of steep chains framing marshy plateaus (Figure 1.4). There are several other high mountains and plateaus surrounding the area, such as Mugenze, Buluku, Ibuga and Narubuye, Mikonzi and Kalira, whose elevations go up to more than 2 km. Two types of reliefs (Graben and Appalachian types) have been recently elucidated in this area, where fault mirrors show via displacement markers, some raised (Horst) and collapsed compartments (Graben) as well as horizontal movements. These faults give rise to the escarpments resulting from vertical and/or horizontal dislocations.

The area is crossed by 2 major rivers. Musheke and Kadubo Rivers, which drains all the water westward into the Ulindi River, one of the main tributaries of Congo River. Other small rivers include Irongero, Karhendezi, Kashwar, and Madubo Rivers (Erick *et al*., 2010).
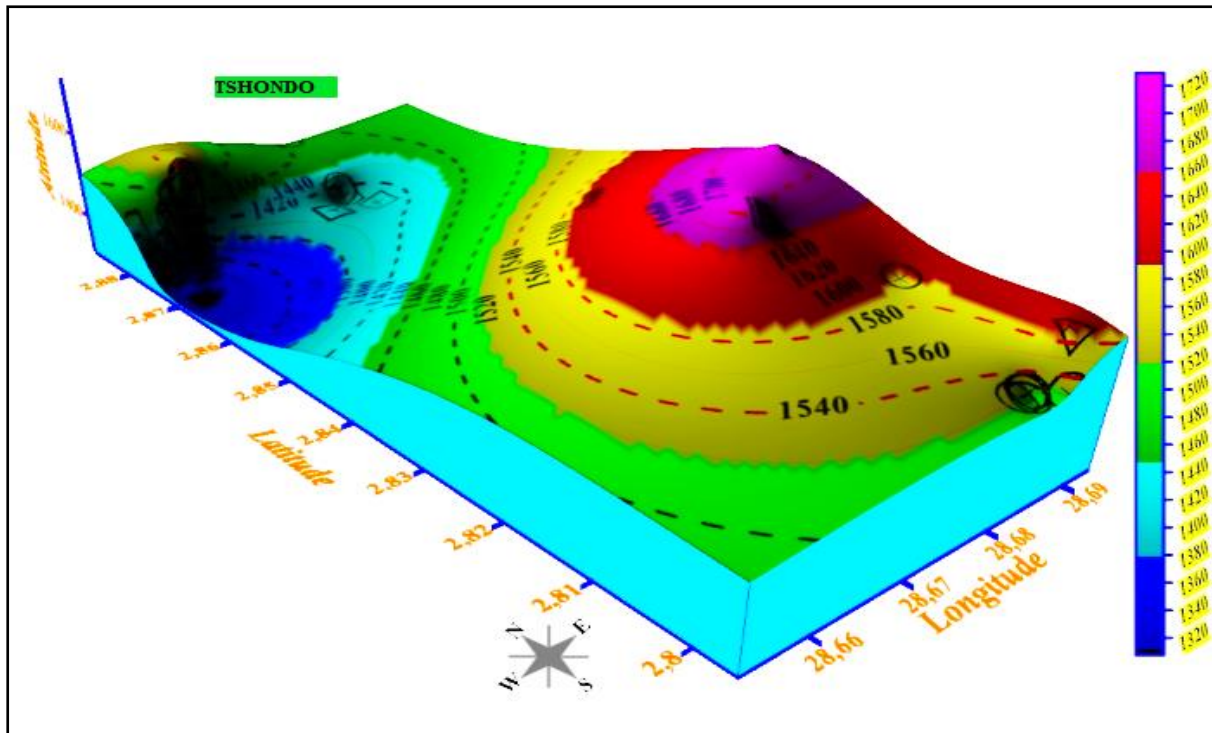
Figure 1.4 : Physiography of the study area (3D view).

1.3.5 Soil

The description of soils at Tshondo is complicated and not well documented. This complexity stems from the variety of rocks, the physiography, and the climate. The studies carried out in this area regarding soils are few in numbers. Two of them are related to Fizi and Uvira zones, respectively, in Ruzizi and Kilombwe valleys (Burrette, 1953, Germain *et al.,* 1955). The soils in mountainous areas with often very rugged relief like Tshondo, offer some superficial dry soils, characterized by an abundant presence of residual quartz. These soils derive from ancient rocks that have very variable characteristics depending on the bedrock and the climate under which they evolved. Mostly, the soils in the Neoproterozoic belt of South-Kivu are classified as follows:

- Well or very well drained soils : Blackish Sandy-clay or reddish-brown to gray-brown, silty.
- Brown Sandy-clay, very dark to black-reddish, very dark-gray sand, finely punctuated. with reddish grains, blackish brown sandy-loamy-clay.
- Insufficiently drained soils : Sandy-silty-clay.
- Undrained soils : Silty-clayey to sticky clay, peaty, and floating.

1.3.6 Surface and Groundwater Resources

The surface water resource at Tshondo is dominated by the Kadubu River and its tributaries (Kashwa, irongero, Mudubwe, Musheke, etc.). This river flows from East to West. The water system is experiencing water spoliation by artisanal miners. No previous surveys have been undertaken to elucidate the groundwater resources in this area, less still throughout the whole Itombwe. However, several groundwater tables are distributed all across the area. The Neoproterozoic meta-sedimentary formations are permeable in some places and constitute somewhat major aquifer reservoirs.

1.3.7 Seismicity

Earthquakes are being frequently felt in the study area. The South-Kivu rift region belongs to the East African rift system. It is the one of the most inhabited regions of Central Africa and the most vulnerable to geohazards. In the 1950's, the first seismic network was installed at Lwiro, along the shore of the Kivu Lake by the "Institut pour la Recherche Scientifique en Afrique centrale" (IRSAC) (De Bremaeker, 1956, 1959, 1961). The latter, in collaboration with Sutton *et al.* (1958), deployed the first seismological data from the IRSAC stations to characterize the seismicity in the region. The first instrumental catalog was hence issued for the period of 1956-1963 but revised later on by Turyomurugyendo (1996). Based on this catalog, Zana *et al.* (1992) quantified the seismic hazard in the region from 1909 to 1980, and produced a map of earthquake risk relying on the distribution of each earthquake magnitude. Since very recently, guided by the evolving knowledge of active tectonics and paleoseismic studies, Delvaux *et al. (2013)* produced a new catalog of instrumental and historical seismicity as shown in (Figure 1.5).
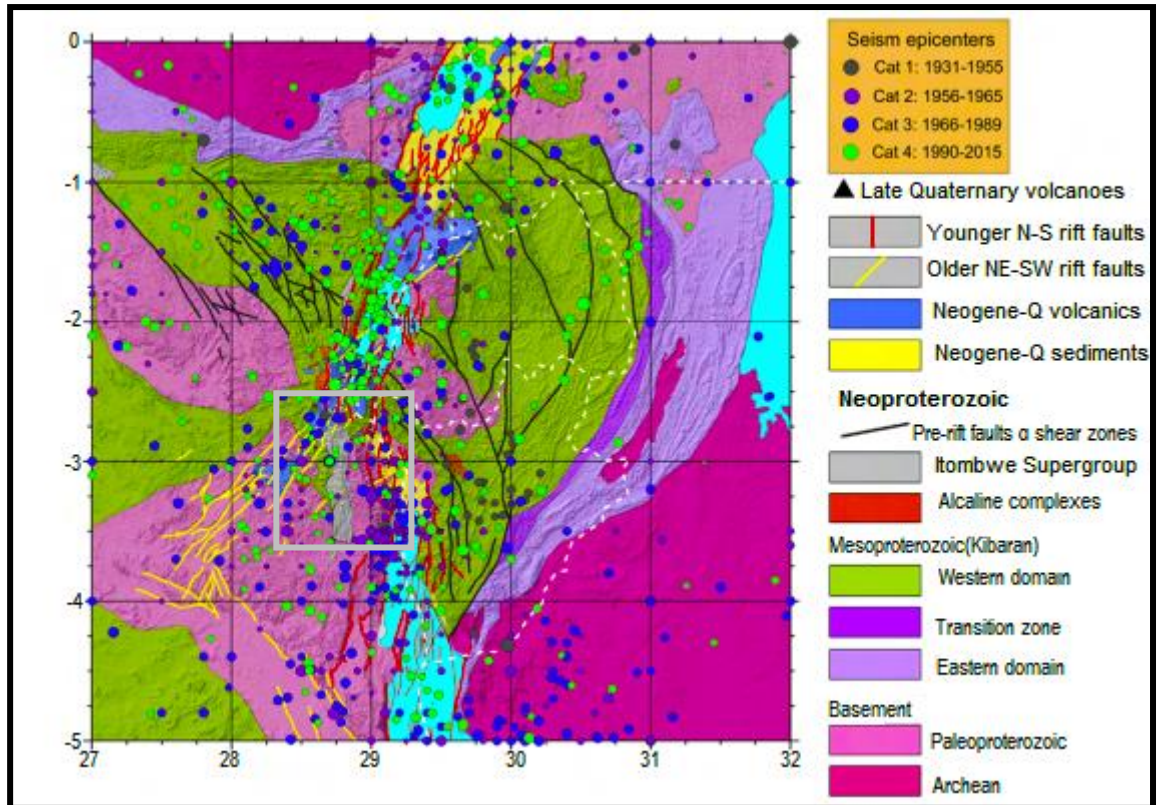
Figure 1.5 : Seismic catalog compiled for the Kivu region and the study area between 1931-2015 (1154 data), after Delvaux (2015).

1.4   THE RESEARCH OBJECTIVES

Driven by the need to give a broad and clear understanding of the slope stability issues, the aim and objectives are as follows :

1.4.1   Main objective

To assess the stability of slopes in the Upper formations of the Neoproterozoic belt of South-Kivu.

1.4.2   Specific objectives

a. To establish the tectonic evolution of Tshondo area.
b. To evaluate the influence of fractures on slope stability in the area.
c. To determine the effect of material propreties on the factors of safety in the area.

1.5   SCOPE OF THE RESEARCH

This work uses both geological and geotechnical surveys to determine how the tectonic evolution, the geological structures and the geotechnical factors are influencing the stability of

slopes in the study area. Tshondo covers an area of 20 km^2, but due to the inaccessibility of certain sites, experiments have been conducted on the slopes listed below. (Table 1.1).

Table 1.1: Location of the investigated slopes.

Experimental Slopes	Location	
	Longitude	Latitude
Slope 1	028.65689°E	-2.875430°S
Slope 2	028.659485°E	-2.87791°S
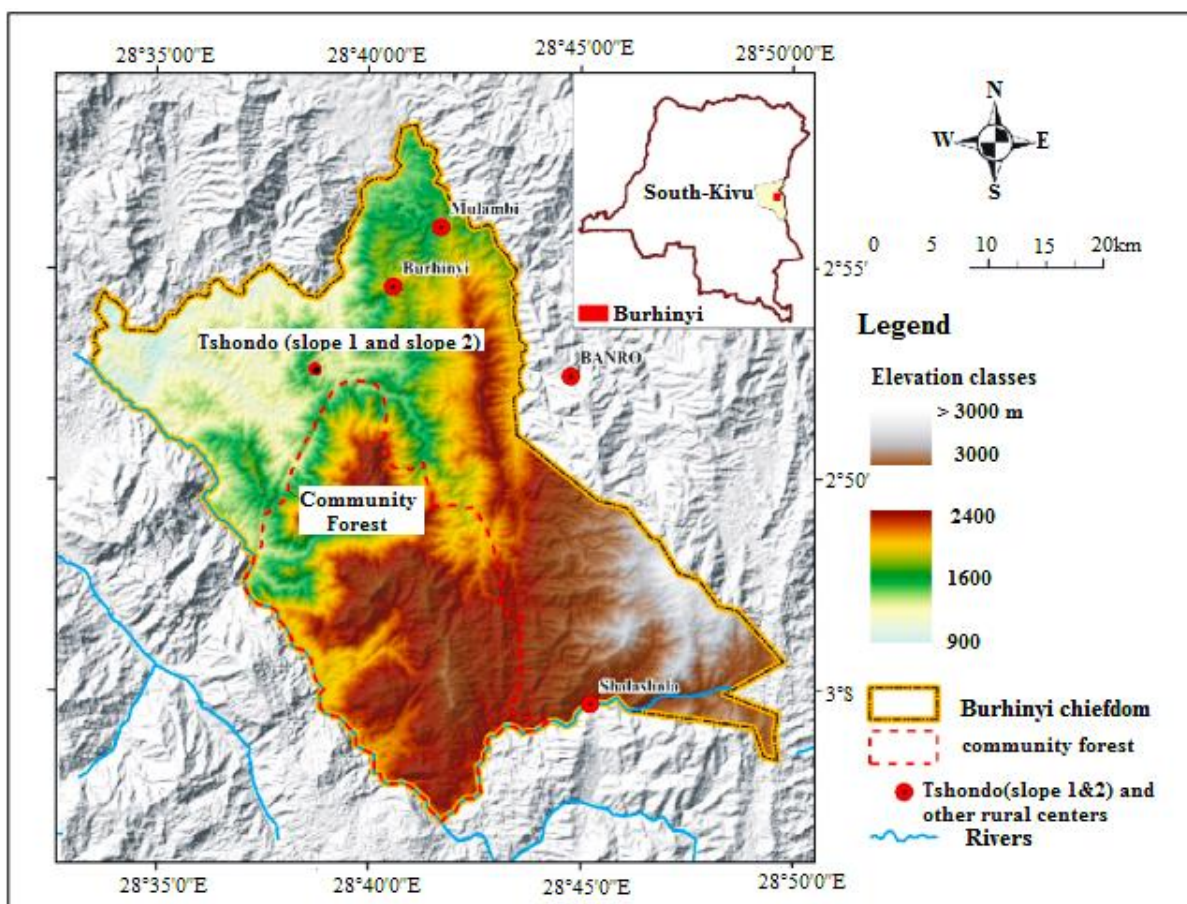
Figure 1.6 : DEM showing the global aspect of the study area.

1.6 JUSTIFICATION AND SIGNIFICANCE

For long period of time, the studies carried out at Tshondo by some researchers only focused on the geological aspects. Mass failures are taking place in the area, endangering people's lives and increasing the environmental degradation. There is a need for integrating the geological knowledge to the concept of slope stability, especially since it has been proven by Munyololo

et al. (1999) that in South-Kivu, mass wasting is not only governed by exogenous causes, but also by endogenous ones. Being a polycausal phenomenon, the stability of slopes requires a more sophisticated approach which analyses efficiently each cause. Paleostress analyses combined with limit equilibrium methods, have appeared to be very powerful tools for the determination of the relationship existing between the tectonic evolution, the earthquake shaking (pseudostatic analysis)**,** the fractural patterns, the soil and rock properties and eventual instabilities (Ogbonnaya, 2016*)*. It is intended that this research will help mining compagnies willing to operate at Tshondo in designing open pit slopes and monitoring slope failures. Furthermore, the research will help raise local community's awareness of slope stability issues in order to minimize the dangers and restore the environmental balance in the area.

1.7 OVERVIEW OF METHODOLOGICAL APPROACH

The approach applied in this research is summarized in the figure below (Figure 1.7). The procedure involved: The formulation of the research problem as a vital function to providing criteria of evaluation, the definition of research objectives as milestones that we wanted to achieve, the identification of gaps via an extensive literature review, the planning of a conceptual structure of the research according to its purpose, field and laboratory investigations , data analysis using different computer software (WinTensor 5.8.6, Geoslope/Slope-W 2018, ArcGIS/QGIS), summary of the results and discussion of each, relying on previous studies, and finally the conclusion and the recommendations.
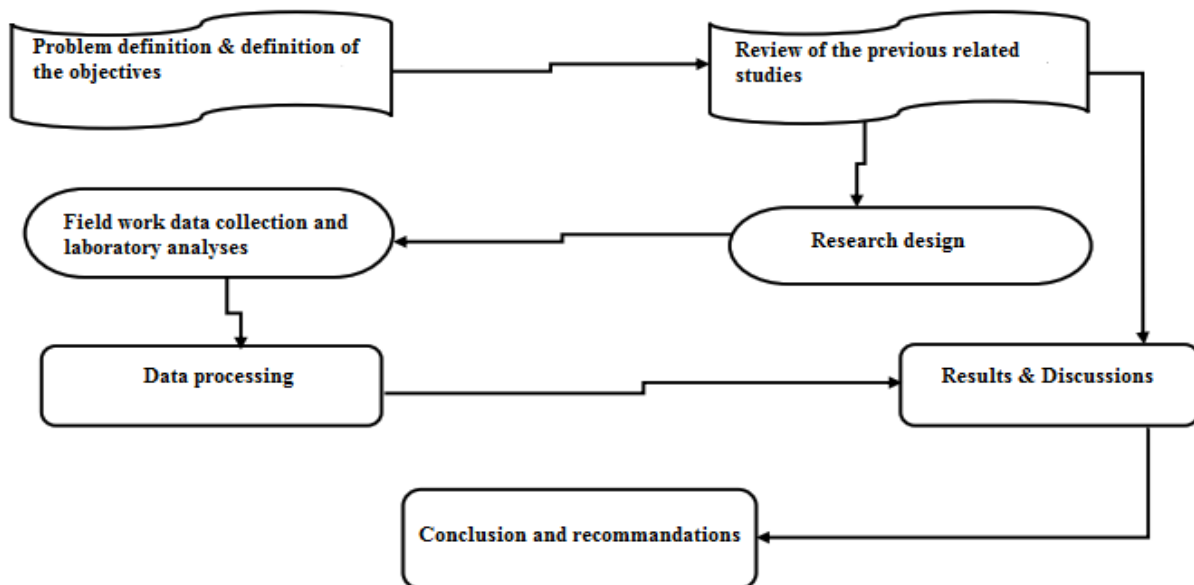
Figure 1.7 : Flow chart exemplifying the stages of research.

1.8   DISSERTATION LAYOUT

Chapter One: provides an insight on the theoretical background information underpinning the study area, the state of the problem, the objectives, the overall methodological approach of the research, and the general layout of this dissertation.

Chapter Two: Gives a global view of the previous works and outlines certain gaps.

Chapter Three: Highlight the methods and the materials used to achieve the objectives assigned to this research.

Chapter four: Presents the results and discussions of the data.

Chapter five: Provides the conclusion and the recommendations.

CHAPTER 2 : LITERATURE REVIEW

2.1   GENERAL INFORMATION

The geo-environmental issue analyzed has been witnessed at Tshondo, but so far it has never been a subject of research. Earlier, between 1945 and 1959, the government, together with the Belgian authorities, have been concerned by slope stability and erosion issues in the region. In their mission called "Mission anti-érosive", they undertook soil conservative measures to prevent these phenomena but unfortunately, the technique was unsuccessful. They only succeeded to stop soils from collapsing. Twenty years later, Lambert (1981) fully realized that the problem was mass wasting such as landslides, rockfalls, and debris flow. After speculations, based on Cahen (1954*)* findings and a detailed cartography, Munyololo *et al.* (1999) suggested a hypothesis of tectonically induced mass wasting in the region. They recognized the presence of a double and apparently a seismotectonic fault with Tanganyikan and Albertian trends (respectively, NW-SE and NE-SW). These faults are associated with the fault of Tshondo crossing the study area. What is still not clearly known are the tectonic regimes from which this fault and its associated structures originate, the magnitude of their slip tendency, but also the relative size of resisting and driving forces acting on different slope materials (rock and soil masses).

2.2   GEOLOGY OF TSHONDO AREA

According to Lepersonne (1971), the Kivu region is geologically subdivided into 5 different geological units (figure 2.1) : The Archean basement, the Rusizian belt (Paleoproterozoic) ; The Kibaran belt and its associated intrusions (Mesoproterozoic) ; the Lindian deposits (Neoproterozoic), the Itombwe Synclinorium (Neoproterozoic), the alkaline plutonic alignments (Neoproterozoic) and the Phanerozoic cover rocks (Karoo). The relations between these units are poorly known due to the inaccessibility to the heavy forestry and permanent insecurity arising from the unstable political situation.
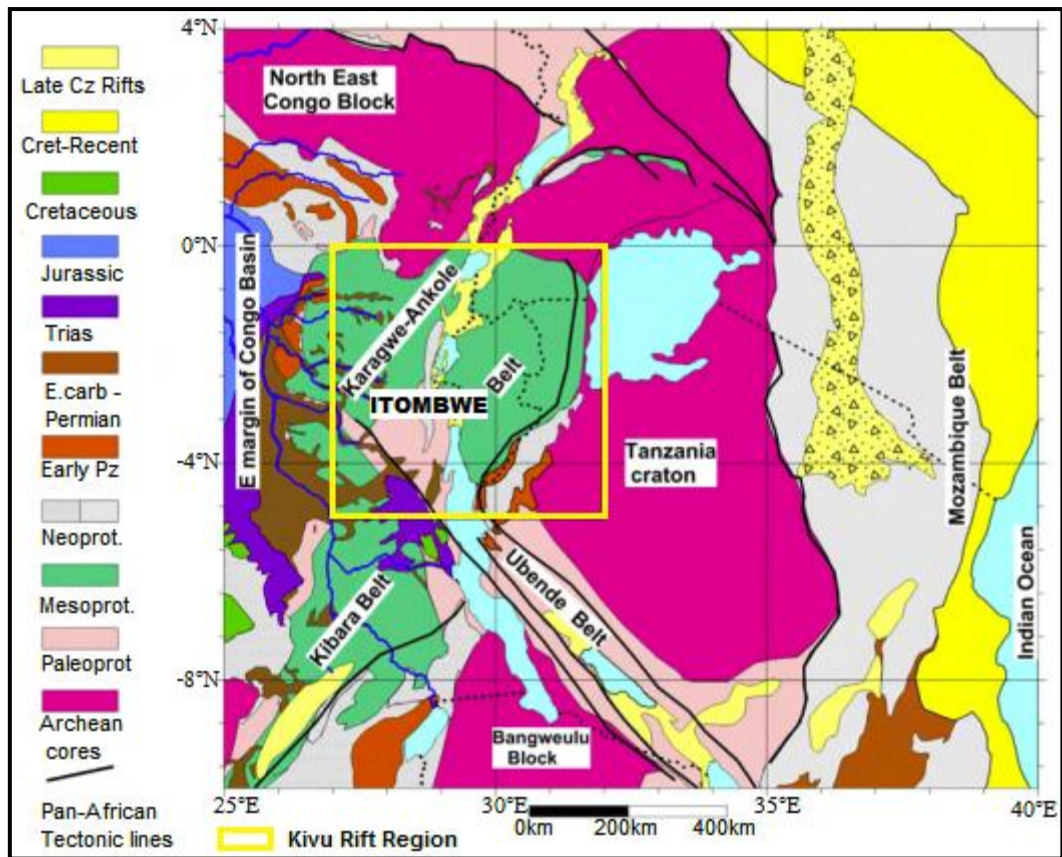
Figure 2.1 : Geological map of the Kivu rift region, after Delvaux (2015).

The Neoproterozoic belt of south-kivu was for the first time studied in 1942 by Lhoest, but his work was published in 1946. The rocks of this belt used to be considered as part of the Burundian (Mesoproterozoic) in the Kibaran belt, but after a meticulous interpretation of Landsat images and geological maps (Figure 2.2), supplemented by field investigations and geochronological data ,they were attached to the end of the Mesoproterozoic between 1310 ± 40 and 648 ± 12 Ma (Villeneuve, 1976, 1977, 1979, 1980, Waleffe, 1988) and the Neoproterozoic between 1020 ± 50 to 575 ± 83 Ma (Walemba, KMA, 2001, Walemba *et al.,* 2004, Villeneuve *et al* ., 2004). The rocks to which this belt is connected are found in various places of South-Kivu region, including Walikale, Bunyakiri (Kampunzu, 1981, Rumvegeri, 1984, 1987), south of the Lake Kivu, Twangiza, Bugoy and Tshondo our study area.
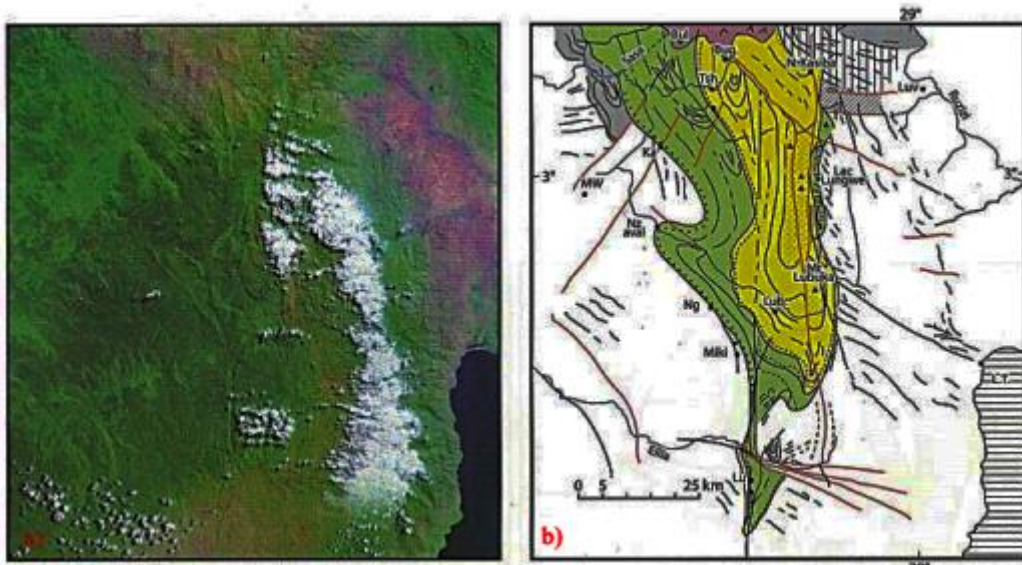
1. Preferential orientation of layers   2. folds   3. Luemba formations   4.Luemba formations   5.Faults   6. lacs   7. Uncorformities

Figure 2.2 : Landsat imagery interpretation in the southern part of the Itombwe area.

On the lithological and stratigraphical points of view, Villeneuve (1987a and 1987b) mapped the geology of the area and evidenced two lithological units: The Lower Kadubu unit, between Kasika and Tshondo, and the Upper Kadubu unit, between Tshondo and Nya-Kasiba. (Figure 2.3). Tshondo area, as exposed in the Itombwe Synclinorium belongs to the Upper Kadutu, in the Tshibangu formations. Villeneuve (1977) classified the rocks at Tshondo as made of black and red sandstones, conglomerates, arkosic sandstones and heterogeneous conglomerates with quartzite pebbles, granites, gneisses and black shales of variable sizes. The heterogeneous conglomerates, reminiscent of glacial deposits were called "mixitites or diamictites".
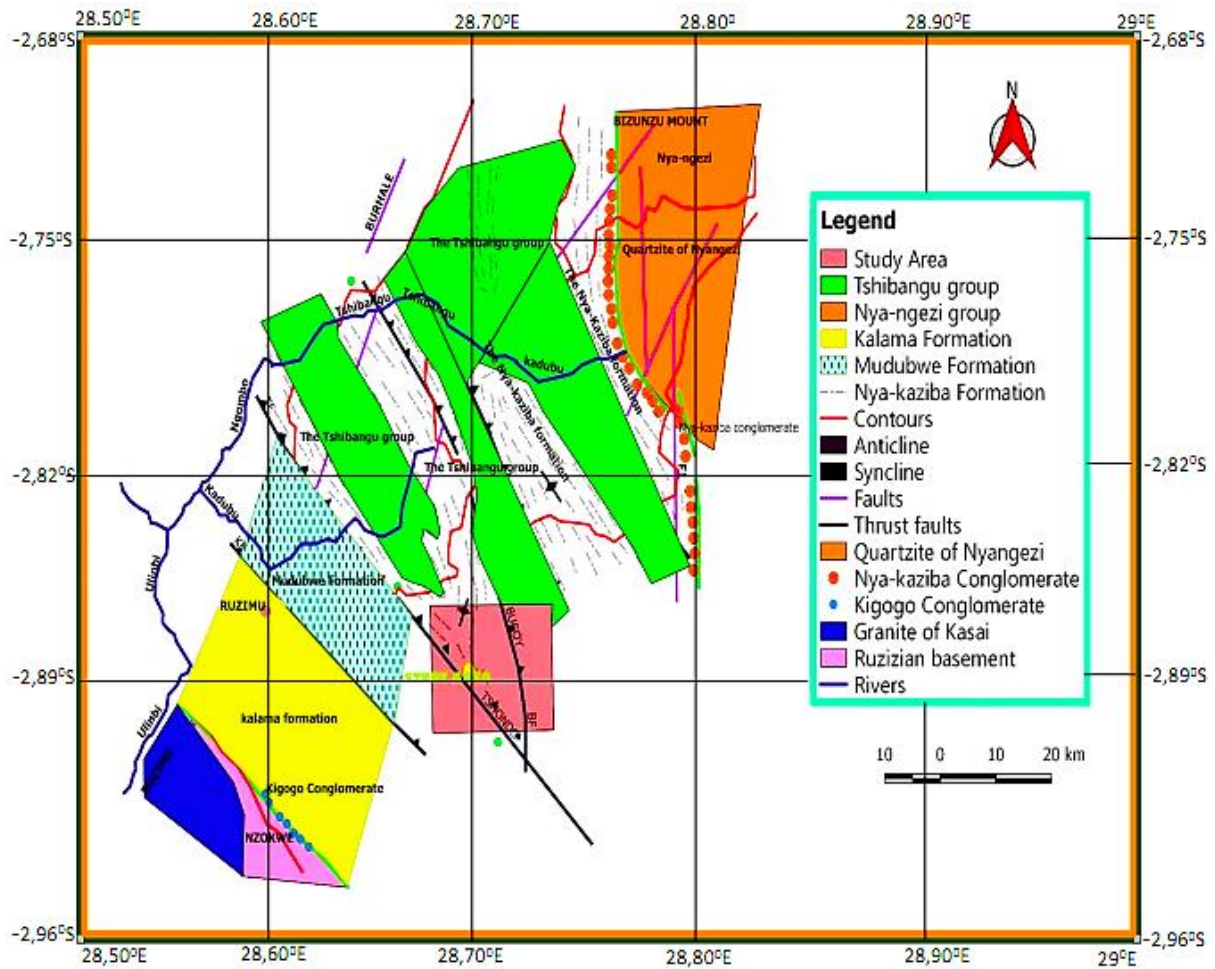
Figure 2.3 : Geological map of the study area.

The first lithostratigraphic correlations known at Tshondo were established by Lhoest (1964) and Villeneuve (1977), but were at some point unreliable and full of controversial discussions because of the faulted contact (materialized by Tshondo and Bugoy faults) between the Upper and the Lower Kadubu. From the analysis of several geological cross-sections established on the basis of the outcrops described by villeneuve (1987), supplemented by the geochronological studies carried out on shales at Tshondo by Walemba (2001), and later on detritic zircons by Kamunzu *et al.* (2004), despite some huge differences in thicknesses, the following lithostratigraphy is accepted. (Figure 2.4).
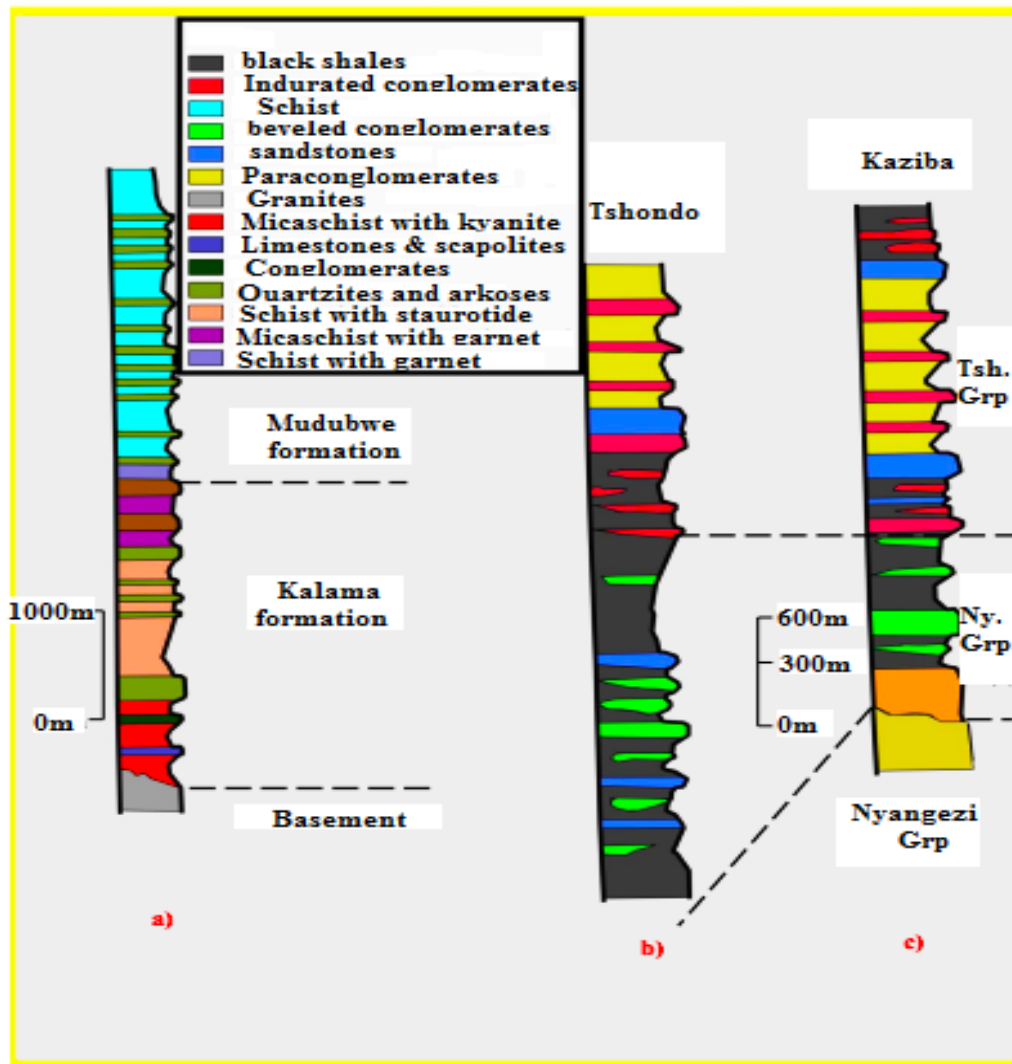
Figure 2.4 : Lithostratigraphy in the Lower (a) and the Upper Kadubu (b,c), after Villeneuve (1987).

On the tectostructural point of view, Lefèvere (2003), Villeneuve (1977 and 1998), Walemba (2001 and 2005) have mapped the geological structures of the area and found them trending N-S, with some virgations towards NW-SE directions. The part of the synclinorium outcropping in the study area is underlined by conglomerate rocks, which disappear in some zones due to the presence of faults. Thus, an angular discordance is not visible everywhere, but mainly on the western limb of the syncline and the southern part of Luemba. Lhoest (1946); Villeneuve (1978 and 1977); Walemba (2001 and 2005) and other pioneers who have conducted some surveys in this Synclinorium have encountered uncertainties, and therefore, multitude interpretations regarding the tectonic events in this zone. Although controversies still exist, most geologists believe, tectonically in three phases of deformation, based on the

clarifications brought by Walemba (2001) and supported by Villeneuve et *al.,* (2004). Apart from the earlier tectonic phases dated of about 1380Ma, which affected the basement, two major compressional phases followed by a shearing phase are recognized:

- **The deformation phase D1 (compressional phase)**

It is characterized by macroscopic and mesoscopic folds, upright to inclined, open to tight, oriented NW- SE with sub-vertical axial surfaces. It is necessary to point out the presence of parasitic folds much tightened, resulting from this phase. At the regional scale, D1 deformation includes Kigogo and Kitwabaluzi anticlines as well as the Ruzimu Syncline.

- **The deformation phase D1-2 (compressional phase)**

Submeridian-oriented structures were generated by phase D1-2. This phase was also able to generate regional folds with schistosity, as well as faults and shear zones. The main stress shortening "sigma 1" is generally oriented E-W. It has also generated the Twangiza anticline and Bugoy Syncline. These folds also include Kahanda, Mohe and Gahinga Synclines, as well as Tshondo and Kasandja anticlines. The phase D1-2 is characterized by tight isoclinal, macroscopic and mesoscopic folds with axial surfaces defined by a preferential orientation of recrystallized micas and quartz grains.

- **The deformation phase D2 (extensional phase)**

It consists of the generation of extensive faults, dextral and sinistral, as well as locally developed shear zones. The shear zones and the extensive faults testify the paroxysmal level of D2. This is the case for Kahanda and Ludjo shear zones, Twangiza faults (NW-SE orientation), Kahanda, Bugoy, Tshondo, and Tshigola faults. These faults dip at angles between 40 and 60°and are being interpreted as the remnants of active faults, initially at a depth of about 2km, but presently, posterior uplifting and erosion have exposed them at the surface. Lefèvere (2003), in his report, integrated remote sensing in the analysis and tectonic interpretation of the Upper Kadubu, and confirmed the presence of several faults crossing the study area, ''Tshondo'' being the principal. On microscopic and megascopic scales of observation, he found that the area is deformed into upright folds towards the W or WSW. The folds were highly strained and truncated by faults that are generally parallel to the overlapping structures. However, reverse movements related to the tertiary rifting might have given rise to some normal resisting faults. Villeneuve et *al.,* (2004), on the other hand, have emphasized that morphologically, the

Itombwe synclinorium in this zone is comparable to a small-graben with a floor sloping towards the W. Some microfolds show a slaty cleavage, with axial surfaces trending NNW-SSE. This cleavage is not permanent and disappears in the sandstones. In thin section, there is a strong deformation of biotites and chlorites in the matrix. Tshondo formations constitute the epimetamorphic domain of the Precambrian of South-Kivu. Its metamorphism is, therefore regional and of low intensity, evolving in the greenschist facies.

The weathering intensity in the Kivu rift region has been quantified by Euduardo *et al.,* (2013). After collecting samples of freshly deposited mudrocks and sandstones upstream and well downstream confluences, and analyzing them by X-ray powder diffraction and X-ray fluorescence, they calculated the CIA (Chemical Index of Alteration) and the WIP (Weathering Index). They found out that the CIA value was lower for sand samples as compared to mud samples, whose WIP value was higher due to lower concentrations of Mg, Ca, N and quartz dilution (Figure 2.5). They concluded that the Itombwe Synclinorium, in the segment between South-Kivu and Tanganyika is marked by an intense chemical weathering (high grade) impressed by a humid climate. In addition, they noted that the concentration of clay minerals in mud samples was responsible for this phenomenon. Kaolinite was found to be > 70 % and sometimes reached 94 % as compared to smectite and illite, even volcaniclastic muds which were relatively in lower concentrations. However, we still need to know the mechanical properties of theses weathered materials in order to assess their impact on slope stability in the study area.
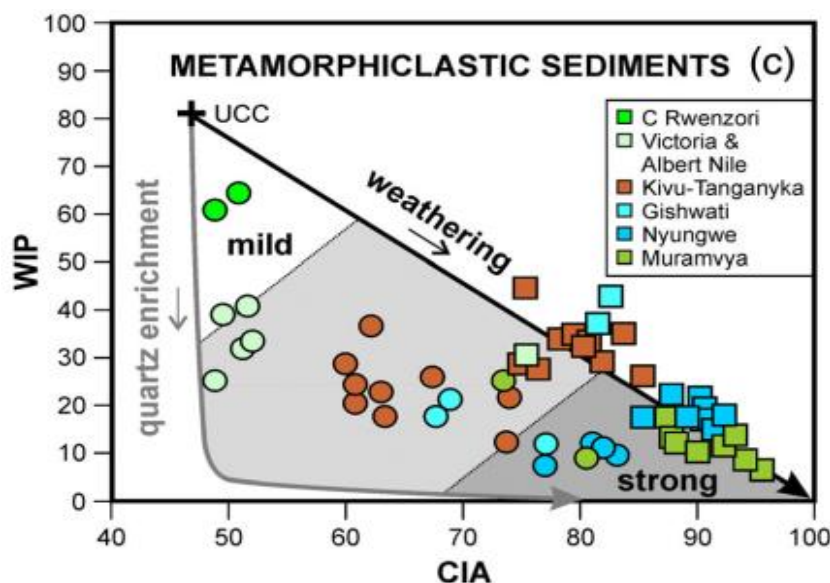
Figure 2.5: Variation of weathering intensity for the metamorphiclastic sediments in the study area.

2.3 BASIC CONCEPTS OF SLOPE STABILITY

2.3.1 Slope components

Basically, the calculations of the factor of safety for any type of slope stability in dry conditions are based on the following factors (Figure 2.6): The cohesion (c), the angle of internal friction (ϕ), the slope angle (β), the area of the block (A) and the gravitational force (w).
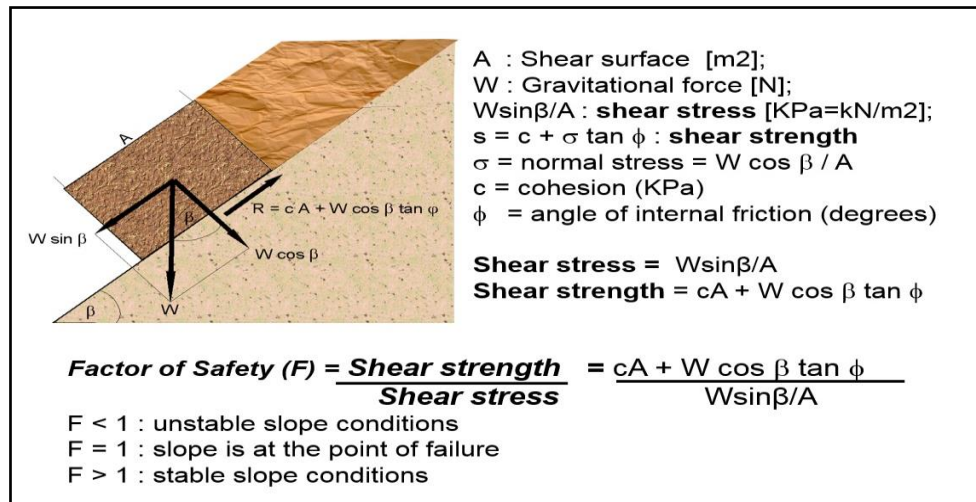
Figure 2.6 : Diagram illustrating the different forces acting on a slope.

Note that this basic equation does not take into consideration the other factors such as, the effect of discontinuities, material properties, groundwater conditions, seismic acceleration, but overall the instability occurs when one of the following components change, as shown in table 2.1. (Cruden *et al.,*1991).

Table 2.1 : Major factors causing slope failure

Increase in shear stress	Decrease in material shear strength
Removal of supports	Weathering
Earthquakes and artificial vibrations	Changes in material structure (fracturing due to unloading)
Increase in lateral pressures	Changes in pore water pressure due to water adsorption & absorption, rising water table

2.3.2   Effect of water on granular vs cohesive slope materials

Granular materials such as sands and gravels have no cohesion. The stability of these types of material is not usually dependent on the effect of water, but more on the friction between particles, reason why they are referred to as frictional soils. The presence of water on granular soils, decrease the effective stress between soil grains, and consequently the frictional resistance. Cohesive soils on the other hand, exhibit significant cohesion when submerged. The amount of water in the soil voids is not influenced by seasonal fluctuations in the groundwater table because the forces of attraction between particles restrain water absorption. However, an increase in absorbed moisture by clay minerals causes the decrease in strength of cohesive soils, especially when these minerals happen to be expansive (Figure 2.7).
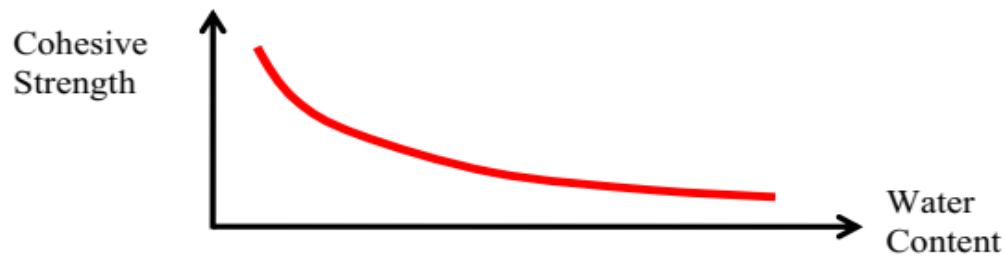
Figure 2.7 : Curve showing the effect of water content on the strength of cohesive clays.

2.3.3   Effect of discontinuities

The presence of tension cracks along the face or crest of a slope can influence its stability. the Investigation in both soils and rocks can be carried out either by boreholes or using some geophysical methods. When the slope is in rock, the discontinuity characteristics have to be keenly determined. Such information can be obtained by boreholes, but also by mapping yexisting outcrops or using existing shafts and pits. The quantification and the analysis of such data is done using a stereonet or a Mohr diagram as it will be seen later on.

2.4   REVIEW OF METHODS OF SLOPE STABILITY

Conventionally, the methods used in the calculations of slope stability are subdivided into 3 main groups, including stereographic and kinematic analyses, imit equilibrium analysis, and rockfall simulators.

2.4.1   Stereographic and Kinematic analyses

Kinematic analysis is used to apprehend different modes of failure that a rock mass is likely to undergo. This analysis requires an in-depth study of rock mass structure and the geometric characteristics of fractures affecting its stability. The stereographic representation of planar and

linear structures is mostly used for this purpose. It allows a visualization of structural data and facilitates the determination of the kinematic feasibility of the rock mass and statistical analysis of the fracture properties. According to Morris theory, the rock mass fail when the frictional resistance frictional become smaller than the revolved shear stress acting on it bearing plane. Other types of analysis can be carried out based on Markland's test described by Hoek and bray (1981). The test shows that failures are likely to take place when the slope face and the fracture dip in the same directions (plane failure), when the line of intersection between two fractures give an inverted wedge and allow release (wedge failure), and lastly when the slope face is parallel to the steeply dipping fracture.
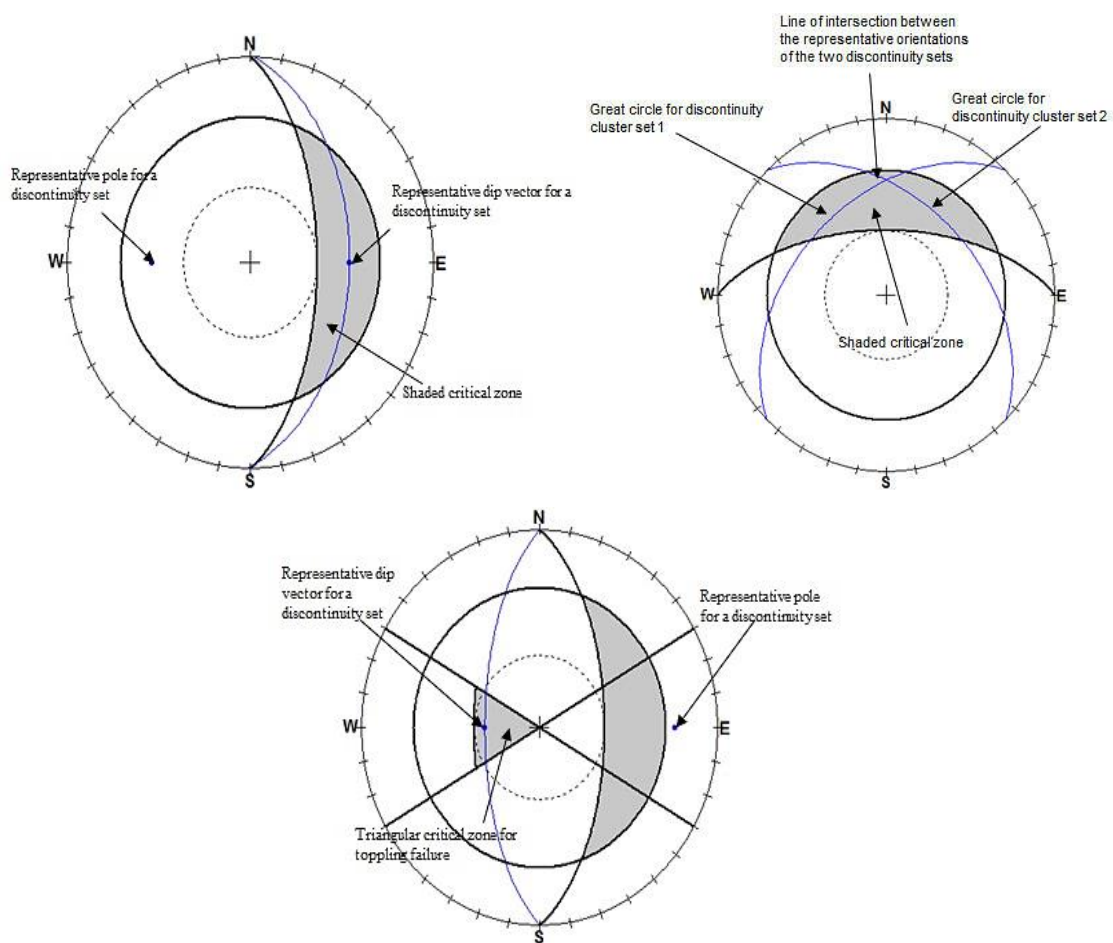
Figure 2.8 : Stereographic plot showing requirements for the 3 different modes of failure in rock masses.

2.4.2   Limit equilibruim methods and limit analysis

These methods analyze the equilibrum of soil and rock masses tending to slide down under the effect of gravity. They all have as output, the determination of the factor of safety, which is the ratio of the shearing resistance to the shear stress needed for equilibrium to be attained.

Theoritically, a slope is said to be stable if FoS > 1, but practically this coefficient is considered as ranging between 1.15 and 1.30 if the following factors are taken into consideration :

- Experimental uncertainties in the determination of material properties,
- Uncertainties related to the influence of tension cracks,
- Errors due to the methods used in the calculation
- The influence of dynamic forces triggered by earthquakes and artificial vibrations.

All limit equilibrium methods assume that the shear strengths of the material along the critical failure surface are governed by linear (Mohr-coulomb) or non-linear relationships between shear strength and the normal shear stress on the failure surface. There are around a dozen methods commonly used in the limit equilibrium analysis. Without making an exhaustive description, some of these methods are:

- Swedish Slip Circle Method of Analysis**: It assumes that the angle of internal friction of soil or rock masses is equal to 0 and the shear strength is assimilated to the cohesion of the materials**
- **Ordinary method of slices (Fellenius method)** : Which is the most used in the category of slice methods. In its original form, it is based on the assumption of an arbitrarily chosen circular slip surface.
- **Simplified Bishop's method** : It neglects tangential forces between slices. The normal forces to the slice bases are obtained by the equation of vertical equilibrium.
- **Morgenstern and Price Method** : It is typically a post-analysis method allowing an expert to explain why an embankment failure has occurred. It is based on the assumption according to which the direction of the interslice forces can be described by an arbitrary mathematical function,
- **Spencer Method** : Which assumes that there is a constant relationship between the vertical and the horizontal components of the interslice forces. This method is similar to the Morgensten-Price Method.
- **Janbu's method** : Which assumes that the interslice normal forces can be defined by their position on a thrust line.

More details about these methods can be found in the works of Duncan (1996) and Espinoza *et al.* (1992).

A more rigorous approach to slope stability analysis is the limit analysis. Unlike limit equilibrium analysis which makes ad-hoc though often reasonable assumptions, limit analysis

is based on rigorous plasticity theory. This enables, among other things, the computation of upper and lower bounds on the true factor of safety.

2.4.3 Rokfall similators

They provide a statistical analysis of the trajectory of unstable blocks. The methods rely on velocity changes as rock blocks roll, slide or bounce on various materials. The Calculations require two restitution coefficients that depend on fragment shapes, slope surface roughness, momentum and deformational properties. Energy, velocity, bounce height and location of rock endpoints are determined and may be analyzed statistically. Remedial measures can be determined using different computer programs based on the kinetic energy and the location of impact on a barrier.

CHAPTER 3 : MATERIALS AND METHODS

3.1   MATERIALS

3.1.1   Materials for literature review

The materials used in the literature review include geological Maps, satelite imageries, Books, articles, administrative documents, academic journals,and conference reports.

3.1.2   Field investigation materials

The data were acquired in the field using a Breithaupt-Kassel geological compass, geological hammer, GPS/Garmin, maps, thermocouple, soil and rock sampling tools (shovel, pick-axe, core-cutters, sample bags, paraffin wax), hand lens,vernier caliper, field notebook, measuring tapes, pencil ,camera, safety boots.

3.1.3   Laboratory materials

The laboratory materials included an optical microscope, drying oven, British Standard sieves, hydrometer, stopwatch, Casagrande apparatus, shear box, soil trimmer, vernier caliper, frictionless end plates and dial gauge.

3.1.4   Deskstop materials

Computer and computer software were applied in this research. Win-tensor software 5.0.2 (developed by Damien Delvaux) and the lower hemisphere of the wulf stereonet were used to analyze the structural data. The software has allowed plotting the data of brittle fractures, the orientations of principal stresses acting on slope surfaces, reconstituting the tectonic evolution of Tshondo area, the regime in which the fractures were generated, and finally estimating the tendency for these fractures to slip (fail). GIS software were used to create new maps and digitalize preexisting ones. Geotechnical software, such as GeoStudio 2018 (Slope/W) was used to analyze the geotechnical data and compute the factors of safety.

3.2   METHODS

3.2.1   FIELD INVESTIGATIONS

The investigations were done in two phases: between July-August 2017 and January 2018. It has basically consisted of observations, measurements, and collection of samples. It was subsidized into 4 steps.

3.2.1.1   Survey of geological structures

The geological features within Tshondo area and on the investigated slopes were observed. Majorly, the survey focused on covering and describing the most favorable zones with

macroscopically identifiable structures, investigating the lithology, and measuring the orientations of rock discontinuities such as faults, fractures, and joints using a Breithaupt-Kassel geological compass (Figure 3.1a). A set of 148 measurements (Strikes and Dips) was collected. Eighty-five on the slopes and sixty-three in the surrounding area (Figure 3.2). The Temperature variations in the hot springs were also assessed using a thermocouple. The maximum and the minimum temperatures were recorded on a daily basis and the global trend was observed (Figure 3.1b).

Figure 3.1 : Orienting fractures (a), and recording spring water temperature at Karhendezi (b).
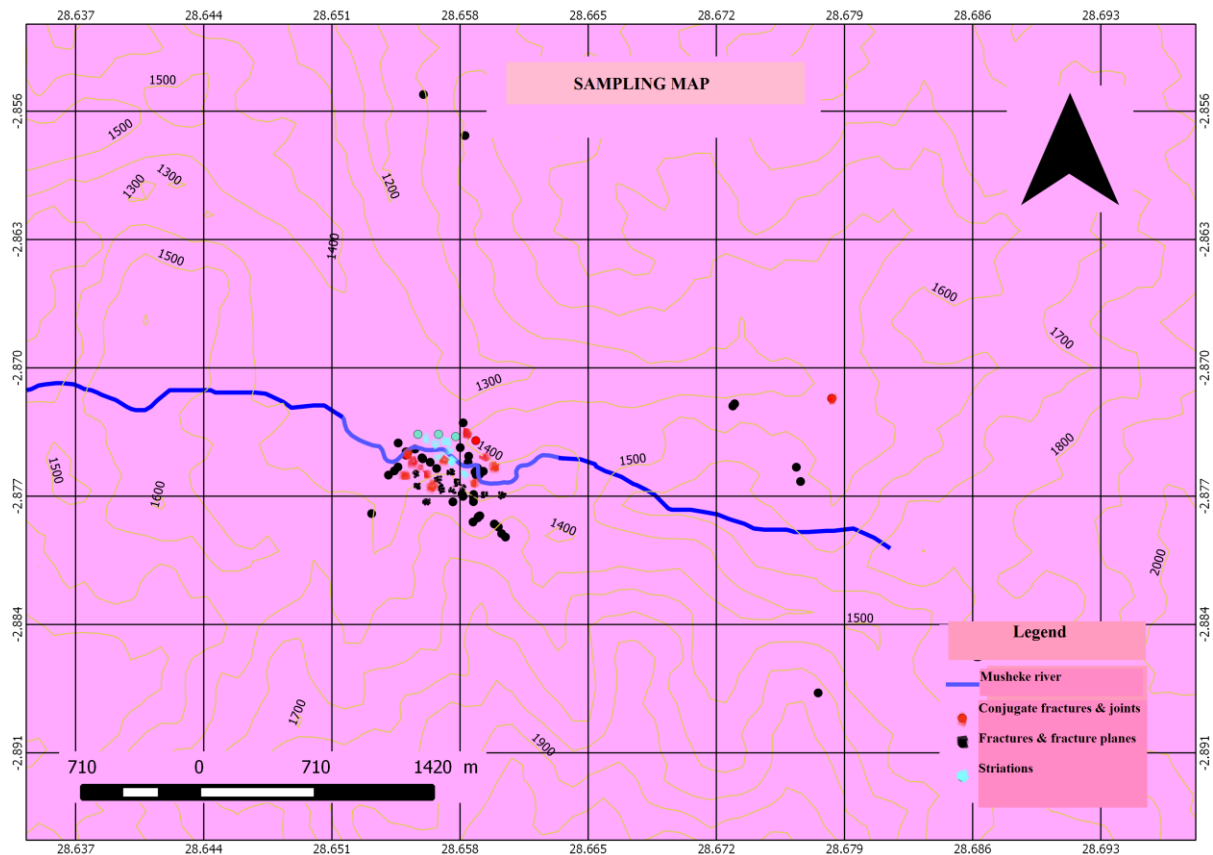
Figure 3.2 : The map showing the sampling points in the study area

3.2.1.2   Geotechnical survey

Due to a limited accessibility of the equipment to the site, we decided to use existing shafts, gullies, and trial pit technique to obtain the information about soil and rock conditions below the surface. Part of the information at this stage is qualitative and was acquired via a visual inspection. The soil and rock horizons of the entire slope profile were investigated and only those parameters which are commonly relevant to slope stability analysis, and allowing an understanding of the geology of the area were described. These include weathering rate, rock names, mineral composition, thickness of different layers, etc.

3.2.1.3   Sampling

Guided by the general geology of the area , soils and rocks were deeply assessed on the two slopes. The sites were chosen based on the representativeness of slopes, the degree of vulnerability and the accessibility. The Landsat images processed and analyzed, showed drastic changes in the state of these slopes from 2003 to present. About 5 kg of heterogeneous soils and 4 rock samples were collected on each slope profile. The soil samples were collected by core cutter methods, following the steps listed below (Figure 3.3).

Step 1: First of all, the cutters were placed on the slopes and pushed vertically into the ground.

Step 2: Secondly, the cutters were removed from the hole very carefully after being dug out using a pick-axe.

Step 3: Lastly, the cutters were wrapped using a paraffin wax, and were labeled.

Figure 3.3 : Collecting soil samples using core cutter method.

Rock samples were collected using logging and hammering methods. The logging methods allowed us to make a detailed record of the geological formations through which the shafts are passing. The hammering method was carried out using a geological hammer, and security measures were taken into consideration. The sampling was done from slightly consolidated to weathered rocks on the slope horizons.

3.2.2   LABORATORY WORK

For the soil and Rock samples collected from the fieldwork, different analyses were conducted in the laboratory of Soil Mechanics, Department of Civil and Construction Engineering at the University of Nairobi. The analyses included: Identification tests, classification tests, and shear strength tests. In addition, a thin section microscopy was carried out in the Mineralogical laboratory, Department of Applied Sciences, at the Official University of Bukavu.

3.2.2.1   Thin-section microscopy

Two rock samples, among the four collected from the slope horizons during the field investigations were prepared and observations have been made. This analysis aimed at

assessing the general composition of the rocks with emphasis on the unstable minerals, such as clay and oxides.

3.2.2.2   Identification Tests

For each of the slope materials, the following analyses were carried out:

3.2.2.2.1   Determination of the Bulk density, Dry density, Water content:

First of all, the test consisted in finding; the weight of the core-cutter filled with undisturbed slope materials; the weight of the core-cutters and the weight of soil were assessed separately as shown in figure 3.4. Secondly, finding the volume of the core-cutter and calculating the bulk density and the dry density using the following formula:

$$\gamma s = Ws/Vc \text{ for the Bulk density,} \qquad (\text{eqn 3.1})$$

$$\gamma d = \gamma s/(1+w) \text{ for the dry density,} \qquad (\text{eqn 3.2})$$

where, γs: Bulk density, Ws: Wt. of soil, Vc: Volume of Core-cutter, γd: Dry Density of Soil W: Moisture content: For the moisture content, 50g of soil was placed in a container and was put in the drying oven for 24hours. After drying, the soil and the container were weighed, and the moisture content was determined as follows:

$$W \% = (W - W_d / W_d - W_c) \text{ x100,} \qquad (\text{eqn 3.3})$$

where, W: Weight. of Container + Wet Soil (W), W_c: Weight. of Container W_d: Weight. of Container + dry Soil, W - W_d: Weight of Moisture, W_d - W_c: Weight of dry Soil

In this test, the height of the core-cutters and their inner diameters for the two slope materials were respectively: 22.8 cm and 10.6 cm.

Figure 3.4: Density and moisture content determination

3.2.2.2.2 Sieve analysis (Grading) and Hydrometer analysis

The sieve analysis consisted in a quantitative distribution of the particle size of soils. In presence of fine-grained soils (0.075 mm to 0.0002 mm diameters), the distribution becomes quite challenging as it is easy to design sieves having very smaller screen size. Therefore, it was good to use the hydrometer analysis for fine grained soils. In the first case, 500g of oven dry soil was transferred to the top of the sieve (arranged in such a way that every upper sieve has a larger opening than the sieve below it). After agitating the sieves, the soil retained on each sieve was transferred to the balance for its amount to be weighed. This analysis has allowed us to determine the composition of the soils (Figure 3.5). In the second case, 50g of soil were transferred into a cup of the mechanical mixer and later on in the hydrometer jar filled with distilled water up to exactly 1000 cc (Cubic centimeter). The soils in suspension were later on roughly mixed by turning the jar upside down and back so as to disturb the sample before the reading can start. Immediately, the hydrometer jar was placed on a table and the stopwatch was launched. At the same time, the hydrometer was carefully placed in the jar and readings were taken in the total elapsed times of ½, 1, 2, 3, up to 60 minutes.

Figure 3.5 :Hydrometer test.

3.2.2.3 Classification Tests

3.2.2.3.1 Atterberg limits

These tests include, the plastic and the liquid limit determination. The tests are used to classify the fine grain portions of a soil.

The **liquid limit** is the moisture content at which the soil behaves less as a viscous fluid and more as a plastic material. By convention, it is the water content, in percent, required in a Casagrandre apparatus along the bottom of a groove to close a distance of 0.5 inches after 25 blows. The procedure used to conduct these tests was as follows:

The soil was moulded wet (200 g of the material passing N0. 36 B.S sieve), placed into a bowl and levelled across, parallel to the base of the Casagrande apparatus. A special tool was then used to make a groove and separate the initial soil into two soil masses. The handle was then turned, and a cam always allow the bowl to fall a predetermined 13mm, twice per second onto a standard hard rubber base. After several turns, the two parts of the soil masses flowed together and joined for at least 25mm. The moisture content corresponding to the liquid limit was determined after 25 blows. However, the procedure was repeated with the addition of little more water to get more moisture content with different number of blows (between 50 and 10 blows).

The plastic **limit** on the other hand, was simply determined by taking a small piece of soil (20g) from the material passing N^0. 36 B.S sieve and gently rolling the soil in order to obtain a plastic

material that can be shaped into a ball. If the soil threads in 3mm thick and just about to break up, then two moistures may be determined, and the average will be taken as the plastic limit.

3.2.2.4   Shear strength tests

Once the soils were classified, it was necessary to determine their shear strength parameters. The shear strengths were also assessed for different slope rock materials. Following are the different tests conducted:

3.2.2.5   Shear strength tests

Once the soils were classified, it was necessary to determine their shear strength parameters. The shear strengths were also assessed for different slope rock materials. Following are the different tests conducted:

3.2.2.5.1   Direct shear test

The test aimed at measuring the variation in soil shear strengths with respect to the load applied normal to the plane of shear. The apparatus used was a shear box made of a rectangular brass. The test was performed systematically in such a way that the soils were cut to fit tightly into a rectangular box (60 mm x 60mm), and the upper toothed grid of the box with its serrations, was placed on top of the sample at right angles to the direction of the shearing plane. Thereafter, a normal load was applied by placing weights (5, 10 and 15 kg) on the yoke for each run of the test. The results from this test were plotted on a Shear stress vs Normal stress graph, and the values of cohesion, together with the angle of internal friction were recorded.

3.2.2.5.2   Unconfined Compressive strength (UCS)

This test was performed in order to estimate the shear strength of cohesive rock materials in the undisturbed state under no confining pressure ($\sigma_3=0$). Four rock materials, including highly weathered pelite and sandstone, completely weathered black shale, and moderately weathered conglomerate were tested. These rock samples were trimmed into suitable dimensions as required by the ASTM and the ISRM. Commonly, they recommended that diameters or lateral dimensions of samples subjected to the UCS test should not be less than 50 mm (Hawkins 1998). For the rock above mentioned, the dimensions were respectively: Highly weathered pelite (50 x 50 x 57) mm, highly weathered sandstone (50 x 50 x 65) mm, completely weathered black shale (52 x 52 x 54) mm, and moderately weathered conglomerate (68 x 68 x 69) mm. These rock samples were loaded axially in a compression testing apparatus (one by one) until they failed (Figure 3.6). Basically, the apparatus was adjusted so that the upper plate contacts the specimen. The initial reading was taken from zero. The loads were then applied mechanically so as to produce an axial strain at a rate of 0.5% per minute. For each observed

strain up to failure, the following parameters were calculated: the axial strain E=L/Lo, the mean cross-sectional area A=(Ao) /1-E and the compressive stress σ=F/A. Graphs showing the relationship between the axial strains and the compressive stresses were represented. From the UCS values were deduced the undrained shear strengths (Su), mostly used in slope stability analysis as the failure in fully saturated cohesive materials often occur in undrained conditions. These values are given by the expression $S_u = \frac{1}{2} q_u$, which is equivalent to the cohesion. In these conditions, the friction coefficient is considered as being zero.

Figure 3.6 : performing unconfined compressive strength.

3.2.3   DATA ANALYSIS

For the structural data, the technique involved relies on stress inversion theories of which two methods are recognized: the classical R-Dihedron methods and the modern iterative Rotational Optimization Method. For the geotechnical data, limit equilibrium and slice methods were involved.

3.2.3.1   Stress inversion technique

This technique was developed based on Bott's (1959) assumption according to which, the slip along a plane take place in the direction of the maximum resolved shear stress, and the brittle microstructures produced by the stress state can be regenerated using the sense and the direction of slip on a sliding plane. The data used in stress inversion are fault-slip data

(slickensides). In Win-tensor program, these data refer to fault planes with measurable slip lines. All the other types of data, which do not show any trace of slip on the slip surfaces are considered as "fractures". To avoid confusion in assessing the relationship between fracture planes and stress axes, the fractures are genetically classified into:

- Tensile fractures (joints, tension gashes, mineralized veins, magmatic dykes), which tend to develop parallel to σ_1 and perpendicular to σ_3.
- Shear fractures (conjugate fractures, slip planes displacing and associated markers), which develop when the shear stress overcomes the frictional line.
- Compression fractures (cleavage planes), which tend to develop parallel to σ_3 and perpendicular to σ_1

3.2.3.1.1 Stress regime determination

The structural data collected from the field were compiled and set in a database in the form of raw data set or pattern. The classification of structural data is based on the bulk organization, the surface morphology, the symmetry and angles between conjugate sets (Delveaux *et al.,* 2003). These are the first step in stress inversion procedures.

For areas or rock masses that have been subjected to successive and intense tectonic events, the raw data set consists of several subsets of fractures. They can be fully described on a mechanical perspective by the stress tensors characterizing the tectonic event. A reliable stress tensor is constituted of subsets made of more than two groups of data of different types and different orientations.

Basically, it is known that a stress tensor is represented by nine numbers which relate the orientation of a plane expressed as the direction of a pole to that plane, and to the traction vectors acting on that plane. However, in microtectonic studies, a full stress tensor is represented by six parameters, but in paleostress inversion, the latter is represented by a reduced stress tensor made of four parameters also known as Euler angles (Guirauld 1989). These are: The ratio R= $(\sigma_2 - \sigma_3) / (\sigma_1 - \sigma_3)$ and the three stress directions, respectively the principal stress axes σ_3 (minimum), σ_2 (intermediate) and σ_1 (maximum). The remaining two parameters of the complete stress tensor are the differential stress ($\sigma_d = \sigma_2 - \sigma_3$) and the mean stress $\sigma_1 + \sigma_2 + \sigma_3/3$ (which basically represent the isotropic pressure pi). (Angelier 1989, 1991, 1994). The stress regime in a given area is defined depending on the nature of the vertical stress axis, the stress regime ratio R, and the stress regime index R' following these conditions : Delvaux *et al.* (2003).

- Extensional (Radial and pure extensions) : When σ_1 is vertical, $0 < R < 0.25$ and $0.25 < R < 0.75$

- Strike-slip (Transtension, pure strike-slip and tanspression) : when σ_2 is vertical, $0.75 < R < 1$ or $1 > R > 0.75$, $0.75 > R > 0.25$ and $\sigma2$ vertical, $0.25 > R > 0$ or σ_3 vertical, $0 < R < 0.2$

- Compressional (Pure and Radial compressions) : When σ_3 is vertical, $0.25 < R < 0.75$, $0.75 < R < 1$

For the stress regime index R' : The stress regimes are given as follows :

$$R' = 2 + R \text{ when } (\sigma_3 \text{ is vertical ; compressional stress regime),}$$
$$R' = 2 - R \text{ when } (\sigma_2 \text{ is vertical ; strike-slip stress regime),}$$
$$R' = R \text{ when } (\sigma_1 \text{ is vertical ; extensional stress regime).}$$

In this study, the four parameters were determined relying on the graphical method well-known as "Right Dihedron Method" developed by Angelier and Mechler (1977). So many improvements have been brought to the method in Win-Tensor (5.8.6) to widen its applicability in paleostress analysis. The method requires to devise the lower hemisphere of Wulf projection into a set of extensional (+ ve) and compressional (- ve) dihedra or quadrants in such a way that σ_1 and σ_3 will lie somewhere between the dihedra on a reference grid of pre-determined orientations. If the direction of these stress axes can be deduced, then the remaining stress axis σ_2 can also be derived from both of them as it is perpendicular to the defined plane.

3.2.3.1.2 Reactivation and failure analysis

Every stress regime is obviously associated with a particular faulting system and can reactivate pre-existing fractures depending on the fault or rock blocs that are likely to slip. One of the basic theories of the kinematic analysis states that the failure under generalized stress condition is predicted by a Mohr-Coulomb yield criterion. The purpose of this analysis is to combine the stress magnitudes in a Mohr-circle and a stereonet so as to predict the fractures lip tendency and discriminate the stable and the unstable ones. This approach relies on Wallace Bott hypothesis which is the foundation of the stress inversion methods commonly used. The reactivation of fault planes, bedding planes, tensile fractures etc. is also of crucial in slope stability assessment. The probability of a given fault to slip or a given fracture to fail can be measured by likening the ratio of normal and shear components of the resolved stress. By defining the sliding friction on a Mohr circle, Jaeger (1969) suggested a condition of reactivation for the pre-existing fractures. The movement occurs if the magnitude of the resolved shear stress exceeds the frictional resistance of a given fracture in the plane. In this analysis, it is usually assumed that all rock masses affected by tensile fractures, joints, faults

and shear zones, possess no cohesion along their fracture planes. So generally, the criterion of reactivation and failure considered is the Navier-coulomb (Figure 3.7).

$$\tau \text{ (critical) }_{mag} = \mu\sigma_{mag}). \qquad \text{(eqn 3.4)}$$

When the pore water pressure is involved, the expression becomes

$$\tau_{mag} = \mu (\sigma n_{mag} - P_f), \qquad \text{(eqn 3.5)}$$

where, σn_{mag}: The magnitude of the resolved normal stress acting on the weakness plane, P_f: The pore water pressure and μ: Coefficient of sliding friction,. This critical stress goes to show that between the shear and normal stresses, there exist a linear relationship resulting in a straight line of slope μ on a Mohr circle, where $\tan^{-1} \mu = \phi$.

Ultimately, the stability and/or the failure of a fault plane, based on the relation above-mentioned is determined by the ratio of shear stress to normal stress. This is what Morris et al (1996) qualified as the "Slip tendency determination". This technique is widely recognized to be a reliable method for predicting fracture instability as well as possible orientations of reactivation. Lisle *et al.* (2004) and Angelier (1990,1994)

$$T_s = \tau / \sigma . \qquad \text{(eqn 3.6)}$$

From the equation (3.7), It can be assumed that the slip tendency is equivalent to the coefficient of sliding friction. This means that the facture that will be more likely to move are the ones with a high ratio of τ /σ, close in value to the sliding friction. The ratio T_s is specific and depends on the friction angle value and the rock properties. It must be expressed by a normalized index of noted T's (Comprise between 0 and 1), which is basically the ratio of the slip tendency and its maximum possible value i.e. the value limited by the slope of the sliding envelope.

$$T's = Ts / (Ts) \text{ max} = \tau \tan \phi /\sigma. \qquad \text{(eqn 3.7)}$$
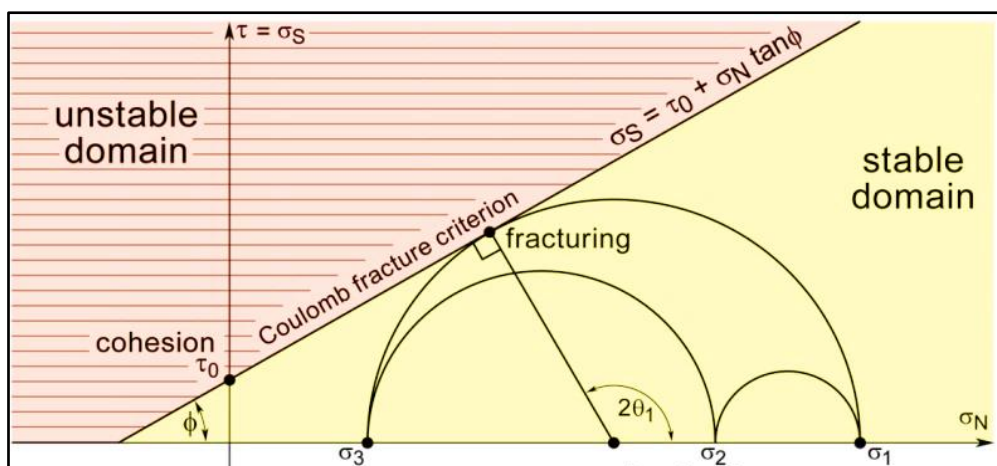
Figure 3.7 : Figure illustrating Navier-coulomb criterion

3.2.3.2 Limit Equilibrium and Slice Methods

The limit equilibrium method helped in determining the global safety factor of slopes using equilibrium forces and moments of each slice. Basically, the safety factor is given by the ratio of resisting to driving forces. Different technique solutions are used for this purpose, they mostly differ in how equilibrium conditions are satisfied between the interslice shear and the interslice normal forces. All these techniques were incorporated in Slope/W Software. Since Bishop's and Janbu's simplified techniques ignore interslice shear forces and only satisfy the moment equilibrium, Spencer and Morgenstern-Price techniques were used in this work as they are the only methods where the factor of safety is computed on the basis of both moment and interslice shear forces. Slope/W is based on the principles of limiting equilibrium. This means that on a free body diagram, forces are represented in such a way that they will remain stationary i.e. the summation of horizontal and vertical moments, will be zero.

The method of slices broadly consists of discretizing the trial slip surface into slices and resolving the factor of safety for every single slice. The normal and shear forces act slice sides and slice bases (Figure 3.8).
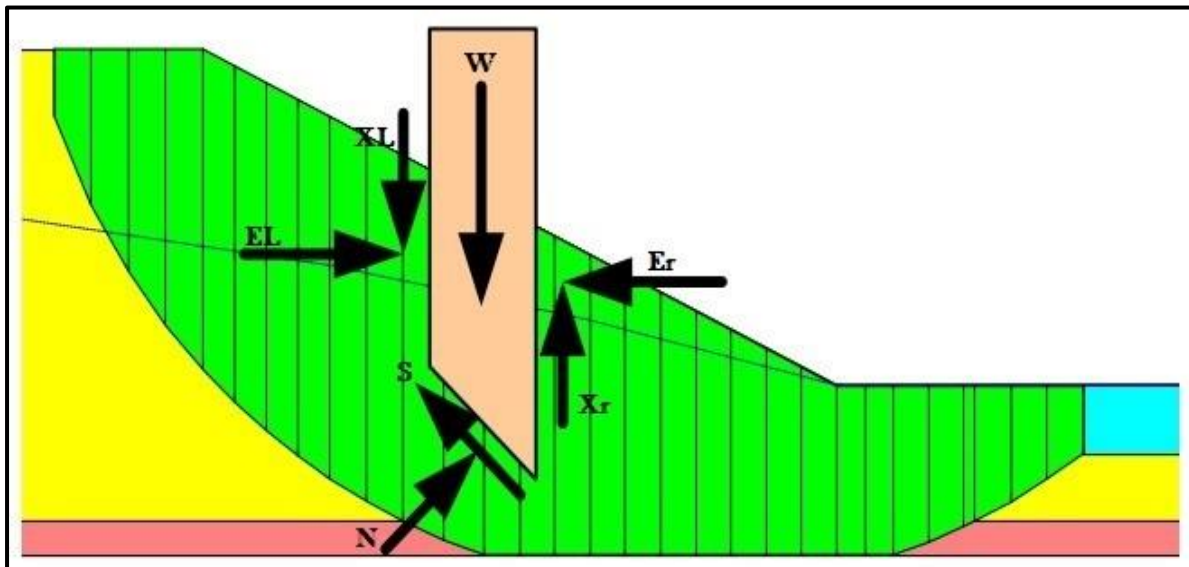
Figure 3.8 : Forces acting on different slices of a sliding mass.

W: weight of the slice, X_L and Xr: Shear forces (Right and Left), E_L and Er: Normal forces (Right and Left), S and N: Shear and Normal forces acting on slice bases.

The General Limit Formulation (GLF) relies on two factor of safety equations. One equation gives the FoS with respect to the moment equilibrium (Fm) while the other equation gives the FoS with respect to the force equilibrium (Ff).

$$F_m = \frac{\sum (c'\beta\ R + (N-u\beta)\tan\phi')}{\sum Wx\ \sum Nf\ \sum Dd}\ , \qquad\qquad \text{(eqn 3.8)}$$

$$F_f = \frac{\sum (c'\beta\ \cos\alpha + (N-u\beta)\tan\phi'\cos\alpha)}{\sum N\sin + \sum D\cos\omega}\ . \qquad\qquad \text{(eqn 3.9)}$$

The terms in the equations are:

C': Effective cohesion, ϕ': Effective angle of friction, u: Pore water pressure, N: Slice base normal stress, W: Slice weight, D: Concentrated point load, β, R, x, f, d, ω: Geometric parameters, α:Inclination of slice base.

3.2.3.3 Seismic considerations using Pseudostatic Approach

The pseudostatic approach is one of the simplest ways of considering the dynamic effects in stability analysis. Basically, the technique requires to specify the earthquake or shaking coefficients K_h or K_v and then apply a portion of slice weight as a horizontal force at the slice centroid such as:

$$F_h = \frac{a_h\ w}{g} = K_h W, \qquad\qquad \text{(eqn 3.10)}$$

$$F_v = \frac{a_v\ w}{g} = K_v W, \qquad\qquad \text{(eqn 3.11)}$$

where: a_h and a_v: Horizontal and vertical pseudostatic accelerations
g: Gravitational acceleration, W: Slice weight, a/g: A dimensionless coefficient K. The coefficients K_h and K_V can be taken as a percentage of g.

In slope/w, for a slope slice, this type of analysis exemplifies the dynamic forces pointing in the direction of the movement on a free body diagram. Before applying pseudostatic seismic load, the shear strength acting on the slice bases should be known. It is deduced either by the mean of Mohr -coulomb failure law or by the undrained strength equation proposed by Duncan et al. (1990). Using pseudostatic analysis in Slope/w is obviously straightforward, but the biggest challenge is knowing which coefficient should be applied. However, it is known theoretically that the value of seismic coefficients acting on a slope should depend on the amplitude of the inertial force induced during the earthquake by the shaking forces, as slope soils are not rigid and the peak acceleration during the seismic activity only last for a short period of time.

CHAPTER 4 : RESULTS AND DISCUSSIONS

4.1 RESULTS OF THE SURVEY OF GEOLOGICAL STRUCTURES

4.1.1 Striae (striations)

These structures were mostly found imprinted on the sliding surface of black shale formations. It is known that faults are discontinuity surfaces affected with a parallel displacement of the surface. The intensity of the displacement vector provides the information on the sense of movement in which a given surface is likely to slide. Orienting these structures, was one of the important steps to acquiring this information. 13 striations have been identified. Others, given their low pronunciation were considered as "probable", and were neglected in the analysis. The considered ones were preferentially trending NE-SW under a mean statistical orientation N040º E / 54º SW and NW-SE for the bearing plane (Figure 4.1). The data can be found in table 4.1.
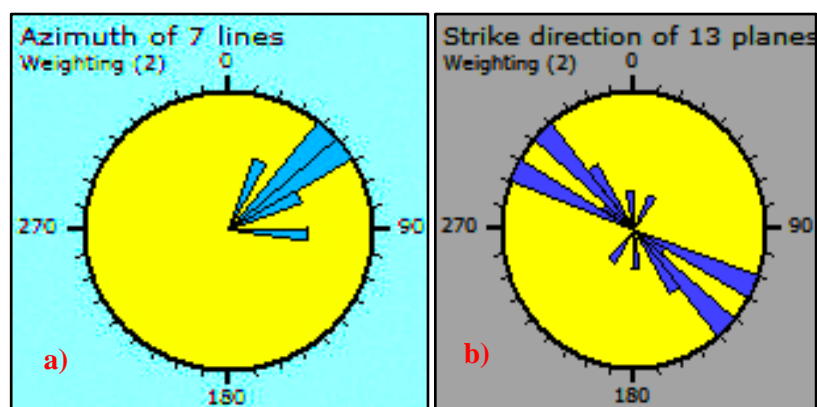
Figure 4.1: Stereonets presenting the preferential orientations of striations (a) and their associated bearing planes(b).

4.1.2 Fractures

After subsetting the raw values, the fracture data, showed a double preferential orientation NW-SE, ENE-WSW, and an average statistical orientation S233º W/73º SE. Conjugate fractures on the other hand, showed three preferential orientations: NE-SW, ENE -WSW and WNW- ESE with an average statistical orientation S218º W/88º NW. (Figure 4.2)
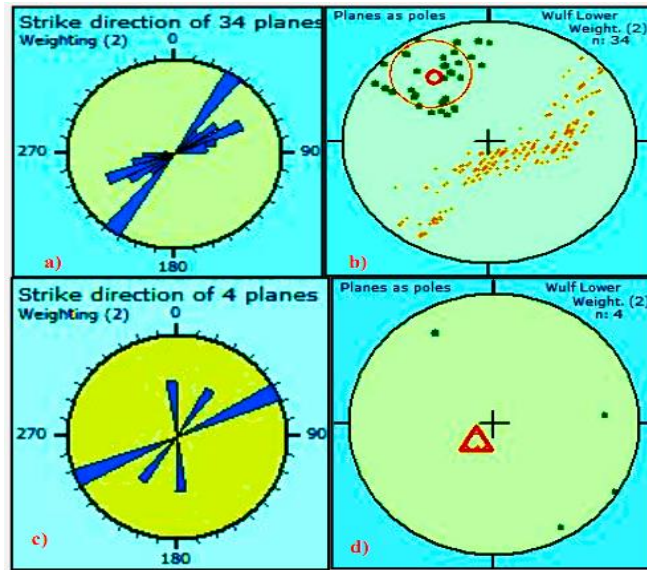
Figure 4.2: Stereonets presenting the preferential orientations of fault and conjugate fractures (a,c) as well as their poles (b,d).

Table 4.1 : Data of striae and bearing planes, collected on slope 1α 2 and their surroundings.

ID	Latitude Y (degree)	Longitude X (degree)	Elevation Z (m)	Dip (striae-bearing plane) in degree	Dip directions (Striae-bearing plane) in degree	Strike (striae-bearing plane) in degree	Observations	Lithology
1	-2.87464	28.65513	1342	033-062	342-052	072-142	Striae	Black Shale
2	-2.87731	28.65761	1340	026-079	305-029	035-119	Striae	Black Shale
3	-2.87731	28.65761	1346	043-079	310-029	040-119	Striae	Black Shale
4	-2.87731	28.65761	1346	044-044	028-026	118-116	Striae	Black Shale
5	-2.87731	28.65761	1347	038-040	057-034	147-124	Striae	Black Shale
6	-2.87731	28.65761	1351	036-040	049-027	139-117	Striae	Black Shale
7	-2.8746	28.65511	1336	059-081	156-231	246-331	Striae	Black Shale
8	-2.8746	28.65511	1336	05-030	223-305	313-035	Striae	Black Shale
9	-2.87435	28.65801	1451	062-064	068-045	158-135	Striae	Black Shale
10	-2.87435	28.65801	1452	063-064	057-045	147-135	Striae	Black Shale
11	-2.87435	28.65801	1453	053-064	095-045	185-135	Striae	Black Shale
12	-2.87435	28.65801	1454	039-040	071-088	185-135	Striae	Black Shale
13	-2.87435	28.65801	1450	064-064	049-045	167-178	Striae	Black Shale

Table 4.2 : Table presenting structural data of faults.

ID	Latitude Y (Degree)	Longitude X (Degree)	Elevation Z (m)	Dip (Degree)	Dip direction (Degree)	Strike (Degree)	Observations
1	-2.87464	28.65514	1340	85	320	50	Fault
2	-2.87464	28.65514	1340	85	305	35	Fault
3	-2.87474	28.6551	1344	63	150	240	Fault
4	-2.87474	28.6551	1344	80	104	194	Fault
5	-2.87515	28.65637	1345	37	175	265	Fault
6	-2.87515	28.65637	1345	75	350	80	Fault
7	-2.87562	28.65441	1336	72	300	30	Fault
8	-2.87515	28.65637	1336	37	175	265	Fault
9	-2.87515	28.65637	1336	80	175	265	Fault
10	-2.87731	28.65761	1454	80	122	212	Fault
11	-2.87731	28.65761	1454	85	122	212	Fault

Table 4.3 : Table presenting measurements of conjugate fractures.

ID	Latitude Y(degree)	Longitude X (degré)	Elevation Z (m)	Dip Fracture A-Fracture B	Dip direction Fracture A-Fracture B	Strike Fracture A-Fracture B	Observations
1	-2.87731	28.65761	1454	85-75	330-265	60-355	Conjugate fractures
2	-2.87541	28.65461	1454	89-78	302-150	32-240	Conjugate fractures
3	-2.87544	28.6558	1453	70-84	80-320	170-50	Conjugate fractures
4	-2.87545	28.6565	1455	85-86	82-330	172-60	Conjugate fractures
5	-2.87538	28.6568	1456	75-86	263-164	353-254	Conjugate fractures

N.B: The summary of data for all other factures can be seen in appendix A 1.

Following are the maps showing the typical pattern of shading for at least a couple of fractures, corresponding to different stress regimes (figure 4.3). These regimes are encompassed in two stereonets as it can be seen in figure 4.4. Note that, the geotectonic map on hill two only represent structures and tensors for different outcrops and sites surveyed. An extrapolation still to be done.
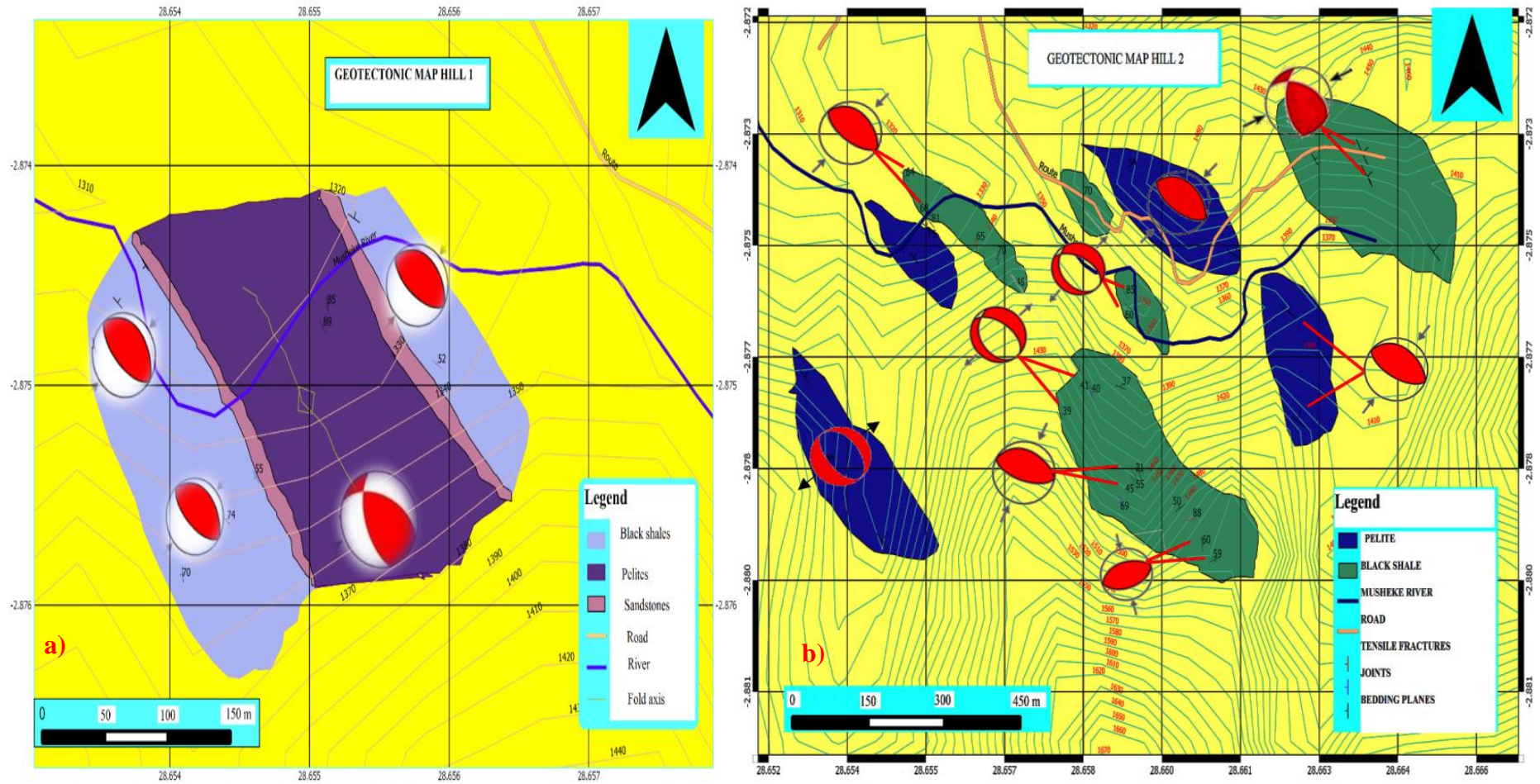
Figure 4.3: Geotectonic maps of the two sloping hills investigated in the study area. Hill 1(a) and Hill 2(b).

4.2 DISCUSSION ON THE TECTONIC EVOLUTION OF TSHONDO

4.2.1 Paleostress reconstitution and tectonic regime determination

The rocks at Tshondo, according to Villeneuve (1977, 1998) and Walemba (2001,2005) were tectonically affected by a Pan-African orogeny, between 1020 ± 50 to 575 ± 83 Ma. This tectonic has reactivated the planar surfaces between adjacent strata into fractures, generally trending NW-SE. Since the area is made of active deformations, it is interpreted that the complex deformation is one of the factors responsible for the occurrence of mass wasting and slope instabilities at Tshondo. It can be seen from the analysis of geological structures that the stress axis orientations and their relative magnitudes were found on the basis of the average orientation of the kinematic axes (P, b and t), but also on the basis of areas of compression and extension of all individual data combined in a single stereonet. For some family of fractures (tensile fractures, conjugate fractures, joints, faults) observed, the orientations of the principal tectonic stresses, which have generated some cracks and led to the displacement of blocs on different slopes and throughout the study area, are such that (Figure. 4.1) : $\sigma_1 \geq \sigma_2 \geq \sigma_3$ (N90º/65ºS, N186º/23ºSE, N250º/9ºSW), but also $\sigma_3 \geq \sigma_1 \geq \sigma_2$ (N44º/17ºSW, N133º/02º NW, N38º/73ºSW). The stress combinations, based on Anderson Theory, require, hypothetically 2 of the 3 principal stresses to be parallel with the surface of the earth material. These conditions are verified for the type of data analyzed as the vertical axes are, σ_1 for one family and σ_3 for the other family. The stress regime indexes (Stress ratios) R'=R were found to be respectively 0.46 and 2.5 (Figure 4.4). We have, therefore 2 regimes (extensional and compressional) corroborating the hypothesis of previous researchers.
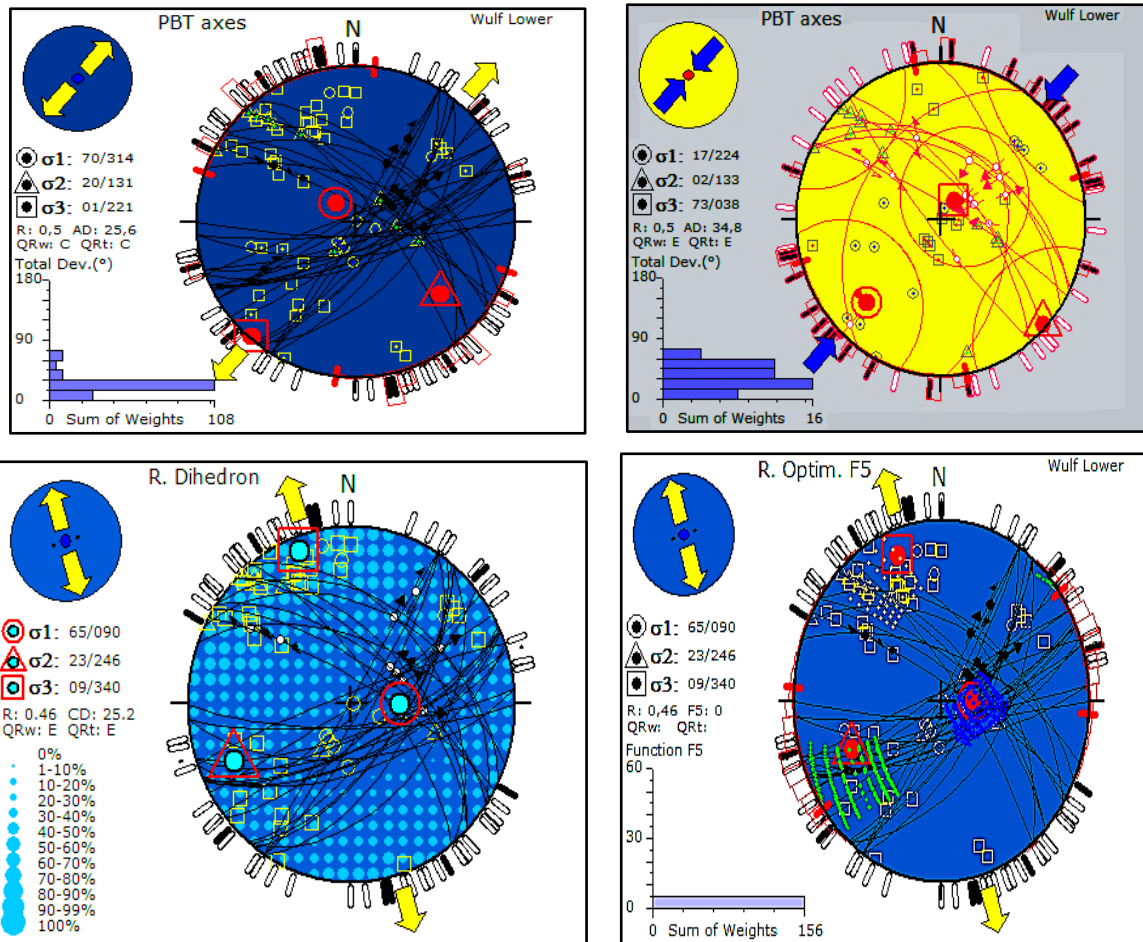
Figure 4.4 : Stereoplots (PBT axes, R.Dihedron and R.Optim Methods) highlighting the preliminary stress parameters for a set of structural data collected on different slopes (Reduced stress tensor, orientation of the horizontal principal stress axes and the stress regime).

It is important to note that both PBT and Right Dieder methods give a direct estimation of the stress axis orientations and their relative magnitudes, but both have to be refined with the Rotational Optimization procedure to produce the approximate results.

Figure 4.5 : Stress regime and stress tensor types from the Anderson deformation theory.

The tectonic regimes thus found allow us to point out the concept of slope tectonics. This term is nowadays justified and its significance has to be recognized as in slope deformation. It is worth mentioning that the stress field on a slope is other than gravity, the result of geological settings created by geodynamic processes, one of those being the active tectonics of the rift system (Figure 4.6). The recurrence of seismic activities (magnitudes 5 and 6 on the Richter scale) witnessed nowadays in the region, have their epicenters located in the SW of Bukavu at the borderline of Walungu and Tshondo. The morphology of the area (marked by a relief of embedded terraces in form of depression), the exponential fluctuation of spring water temperatures in the calcareous concretions at Karhendezi (65-73ºC), are tangible proofs to the existence of active faults and therefore, tectonically induced mass failure.

Karhendezi springs waters, according to a previous geochemical analysis carried out in South-Kivu by Mambo et al. (2008), are of bicarbonate-sodium-type. This stems from a constant supply of magmatic carbon dioxide to the geothermal system, but also the manifestations of the active faults in the unconsolidated areas and favorable conditions for the heat coming from the magma underneath. The high thermal gradient causes heating of waters in the lower basin, while the active faults are draining hot waters to the ground surface. These manifestations only occur in intensively faulted zones, where reactivation of old fractures took place (Patrick M.2015). In microtectonic analysis, these temperatures, together with the geothermometer parameters can be used to indicate the location of basement faults, for which activities may be more recent. It can therefore be concluded that there exist some relationships between the increase in water temperatures, the tectonic fractures oriented in the Albertian and Tanganyikan directions and the slope failures in the area.
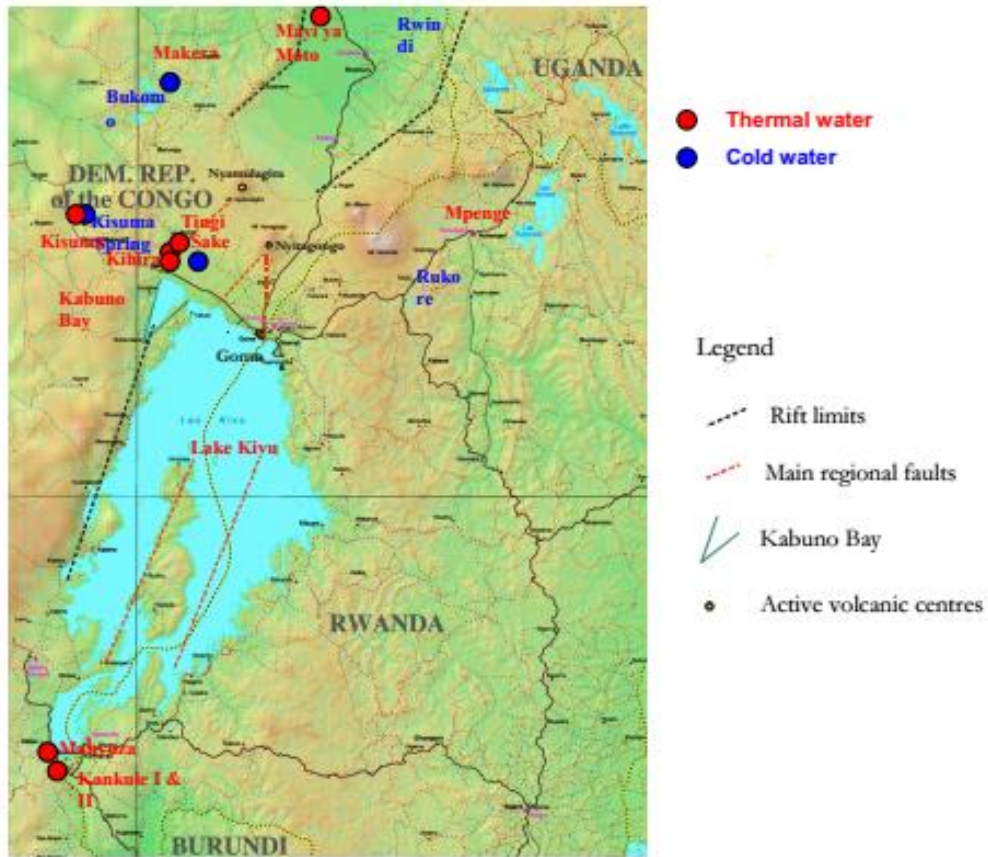
Figure 4.6 : some spring water along the western branch of the East-African Rift

4.3 DISCUSSION OF THE INFLUENCE OF FRACTURES ON SLOPE STABILITY

4.3.1 Reactivation and failure analysis

Generally, the 3D stress tensor is depicted within 3 circles in a normal shear stress magnitude and the areas between the circles define the boundary stress vector acting on the sloping fault planes. The outward circle is the one illustrating the failure and the other two represent the pre-existing fractures. Jaeger *et al.,* (2007) assumed that the magnitude of the principal maximal stress axis σ_1 is equal to 100MPa in extensional and compressional regimes, and the magnitude of the principal minimum stress σ_3 is deduced using the formula: $\psi = \sigma_{3\,mag} / \sigma_{1mag}$. The Revolved stress on a plane, after the application of the stress tensor is expressed with $N_{mag\ or}$ σ_{mag} (magnitude of revolved normal stress on the plane), and T_{mag} or τ_{mag} (magnitude of resolved shear stress on the plane). The friction coefficient $\mu = \arctan(\tau_{mag} / \sigma_{mag})$. It is always good to collect as many structural data as possible, as most of structural inversion methods are statistic. However, not all the data are taken into consideration for the calculation of the failure tendency. Win-tensor program usually select the most relevant data from each subset to determine the slip tendency of the entire set, and consequently its sense of movement.

The probability for 33 representative fractures, undergoing normal and shear stresses to fail is presented by the 3D Mohr diagram as shown below.
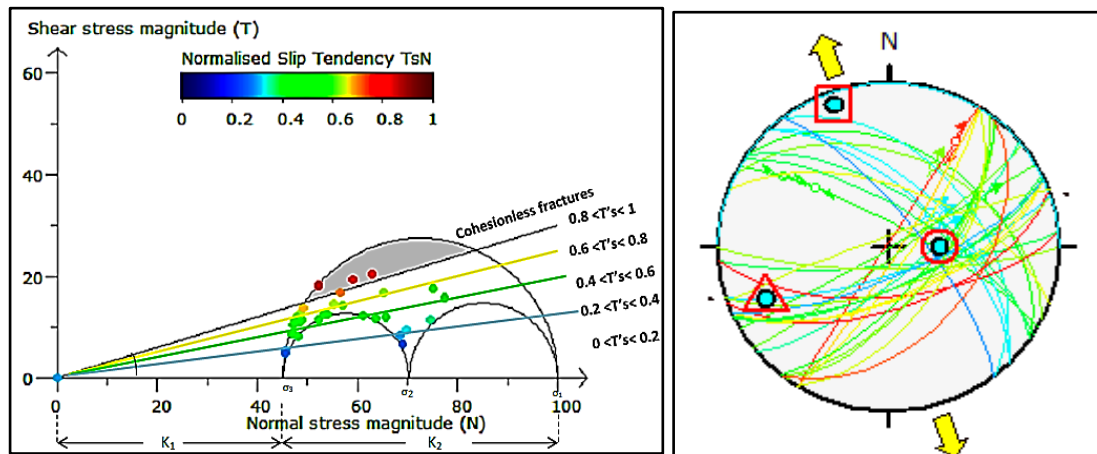
Figure 4.7 : Determination of fracture normalized slip tendencies on a Mohr- coulomb failure diagram with corresponding stereo plot (Only representative data are used).

The stress shape ratios being respectively equal to 0.46 and 2.5, the resulting slip tendencies on the Mohr diagram varies from high to medium values (1-0) on the investigated slopes. The analysis indicates that the maximum slip tendency varies between 0.8 and 1 and the minimum between 0 and 0.2. These values suggest that the set of fractures in red dots (N=4) are above the critical stress. They are no longer stable. They represent all the collapsing fault planes that are promoting slope instability. The yellow and green dots (N= 27), between (0.4 - 0.8), stand for joints, tensile and conjugate fractures. Under the effect shaking or an excessive pore water pressure during a rainfall for example, these fractures will present a higher probability of failure because, the normal stress magnitude will be reduced by an amount equal to the force exerted on the plane, by having fractures and the pore spaces filled by water rather than air when the material is dry or undersaturated. Lastly, the fractures in blue dots (N=2), between (0 - 0.4), represent the bedding planes that are far below the main frictional line and do not influence the instability of slopes that much, because at that point, they are stable.

For these data, we were not able to predict the sense of movement. Admittedly, fault mirrors outcrop on the slopes and all over the area, but unfortunately, they were showing a scarcity of tectoglyphs to characterize the sense of movement. The reason being that all the markers might have been crumbled and erased either by the erosion or by any other climatic agent given the physical properties of the completely weathered black shales on which they are printed. The 13 structural measurements collected for striations are not sufficient to accurately predict the sense of movement for all the fracture planes.

45

NB: Two time series images giving information on landscape degradation at Tshondo for the past 15 years is included in the next session. But, below is a Landsat image showing the study area and how land use and landcover are classified.
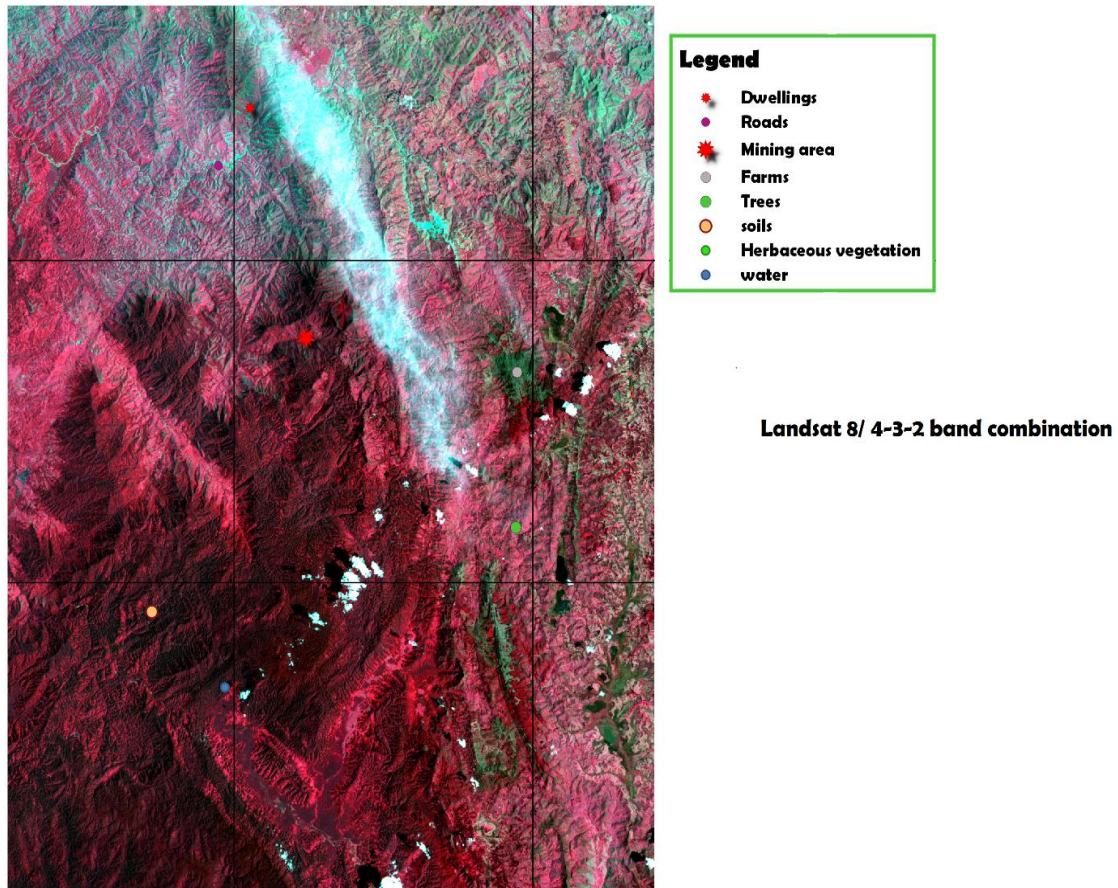
Figure 4.8: A standard "false color" composite / 4-3-2 band combination, showing the land use and landcover in our study area.

As it can be seen from the image, the healthier vegetation appears in red especially in the areas surrounding the mining site. Soils and roads are brown reddish. The dwellings are in green light color, the water is displayed in black color, and the farms are green-darkish, merged with a bit of brown.

Figure 4.9: Google Earth Imagery showing the historical changes at Tshondo. Between 2003 - 2018. Acquisition dates: 27/03/2003 (a) and 12/06/2018 (b).

From the two images, it can be seen that the rate of mass wasting has increased during the past 25 years. The natural vegetation has been removed mostly by artisanal miners, destabilizing the stability of slopes. The soft rocks were dug into furrows, dragging musheke river with them.

4.4   GEOTECHNICAL RESULTS

4.4.1   Slope characterization

The assessed slopes are respectively located on latitudes 028.6568°E, -2.87543°S and longitudes 028.659485°E, -2.87791°S. These steep slopes were subjected to the same type of tectonic stresses, their stratigraphy is broadly made of soil and rock masses with different properties. The geotechnical field investigation showed that 5 meters of the soil are underlaid by completely weathered black shales (4 and 6 m), moderately weathered conglomerates (2m), weathered pelites, similar to sandstones (6 m) in order of increasing depth.

4.4.2   Geotechnical characteristic of soils and rocks

The engineering properties of selected bulk samples, taken from existing gullies and by core cutter techniques were analyzed in the laboratory. The tests have given the following results.

4.4.2.1   Grading and hydrometer analysis (Grain Size distribution)

The engineering properties of selected bulk samples, taken from existing gullies and by core cutter techniques were analyzed in the laboratory. The tests have given the following results.

4.4.2.2   Grading and hydrometer analysis (Grain Size distribution)

The results show that for the two slopes, the soils contain approximately 27.8% and 16.3% (close to 20% if we take into consideration the errors) particle diameters less than 0.075 mm. In Accordance with ASTM D2487 standard, this test needed to be supplemented by a hydrometer test for finer particles as twenty percent (20%) and more passed the No. 200 Sieve. The curves (Figure 4.9 a and b) show that for slope 1: % Sand= 63.2, % Fines= 27.8 and for slope 2: % Sand= 84.7, % Fines= 16.3. D_{60}, D_{30}, and D_{10} are respectively: 2.6 mm, 0.1 mm, 0.024 mm for slope 1 and 1.2 mm, 0.18 mm and 0.026 mm for slope 2. From these parameters, the uniformity and gradation (curvature) coefficients were found as being respectively:

$$C_u = \frac{D60}{D10} = \frac{2.6}{0.024} = 108.3 \qquad\qquad C_c = \frac{(0.1)^2}{2.6 * 0.024} = \frac{(0.1)^2}{0.024} = 0.16 \text{ (slope 1)}.$$

$$C_u = \frac{D60}{D10} = \frac{1.8}{0.026} = 46 \qquad\qquad C_c = \frac{(0.18)^2}{1.2 * 0.026} = \frac{(0.18)^2}{0.024} = 0.48 \text{ (slope 2)}.$$

From these values ($C_u > 6$ and $C_c < 1$), the Unified Classification of soil suggests that these soils are poorly graded (SP) silty sands (SM). There's no good distribution for all the particles.
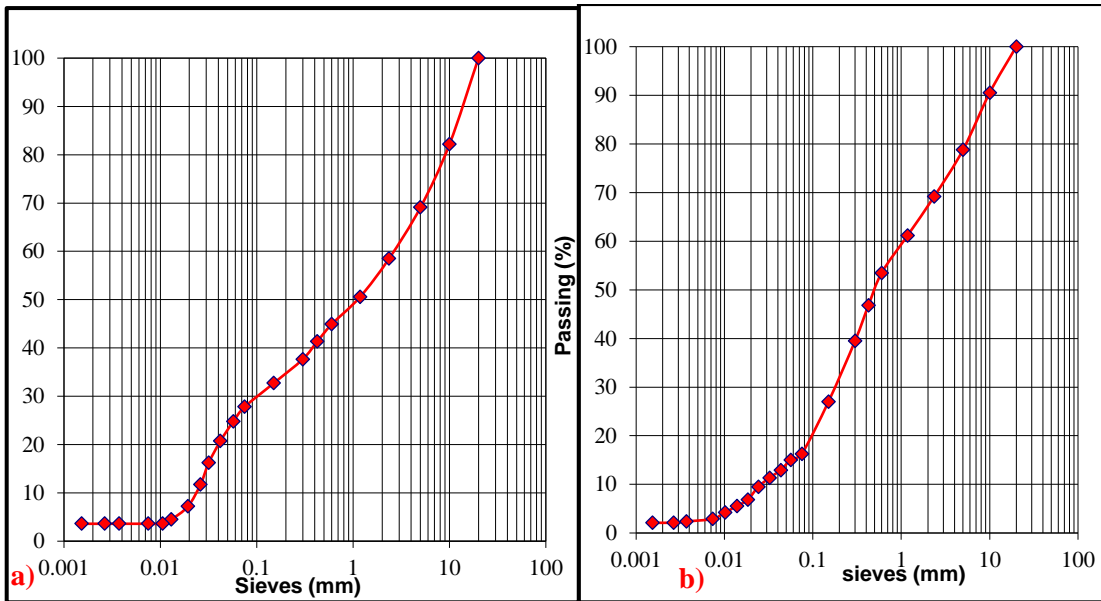
Figure 4.10 : Grading curves for slope 1(a) and slope 2 (b).

4.4.2.3 Atterberg limits

As the soils contained a significant amount of sand as shown in the previous test, the later was removed by passing the soils through the N40 sieve. The test performed on the fine portions of the soils revealed that threads could not be rolled out down to 1/8 inches at any moisture possible. The plasticity index was found to be 0. The soils have been directly classified as non-plastic (cohesionless).
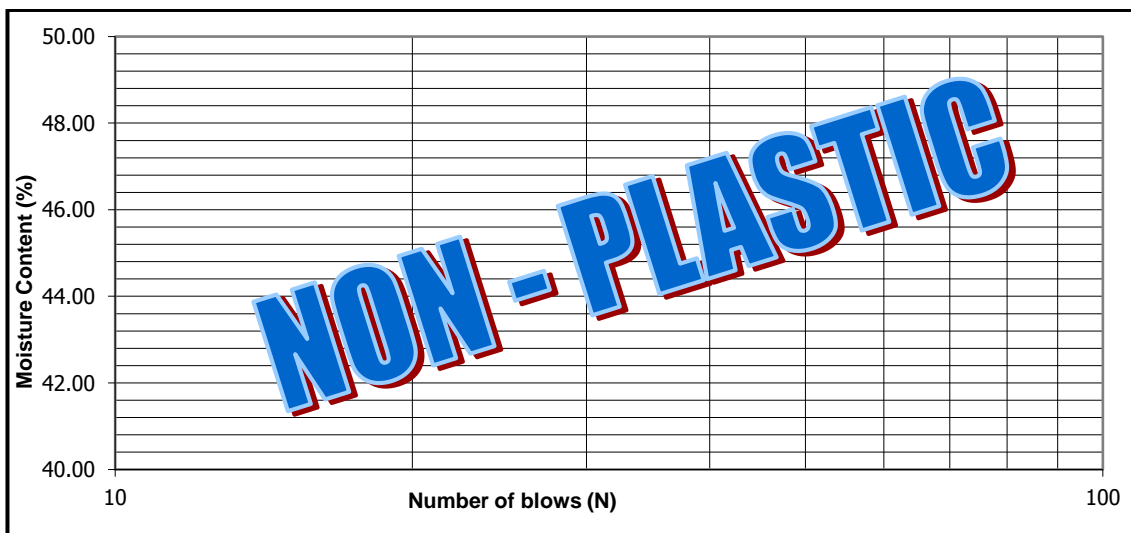
Figure 4.11 : Typical representation of the test results from the Casagrande apparatus (Atterberg limits).

4.4.2.4 Bulk density, water content, and specific gravity

The bulk densities of the soil samples were relatively small (6.92 KN/m^3 for slope 1 and 14.24 KN/m^3 for slope 2). This is due to the fact that, not only the soils contain organic matters and

were formed in carbon-rich strata of black shales, but also, the bonding between the grains is not enough (cohesionless soils). Broadly, the water contents of soils and rocks were ranging between 4 and 27%. The values of specific gravity were respectively 2.553 for slope 1 and 2.59 for slope 2.

4.4.2.5 Direct shear

The maximum shear stresses were measured at consecutively higher increments of applied loads. The shear stresses required to displace the slope materials occurs at 1.5 and 1.52kg/cm^2. By plotting the shear stresses versus the normal stresses, the Mohr-Coulomb failure envelope gave the following strength parameter values: C= 0.01kg/cm² (1.961Kpa), Ø = 26° for slope 1 and C = 0.02kg/cm² (0.986Kpa), Ø = 27° for slope 2 (Figure 4.11).
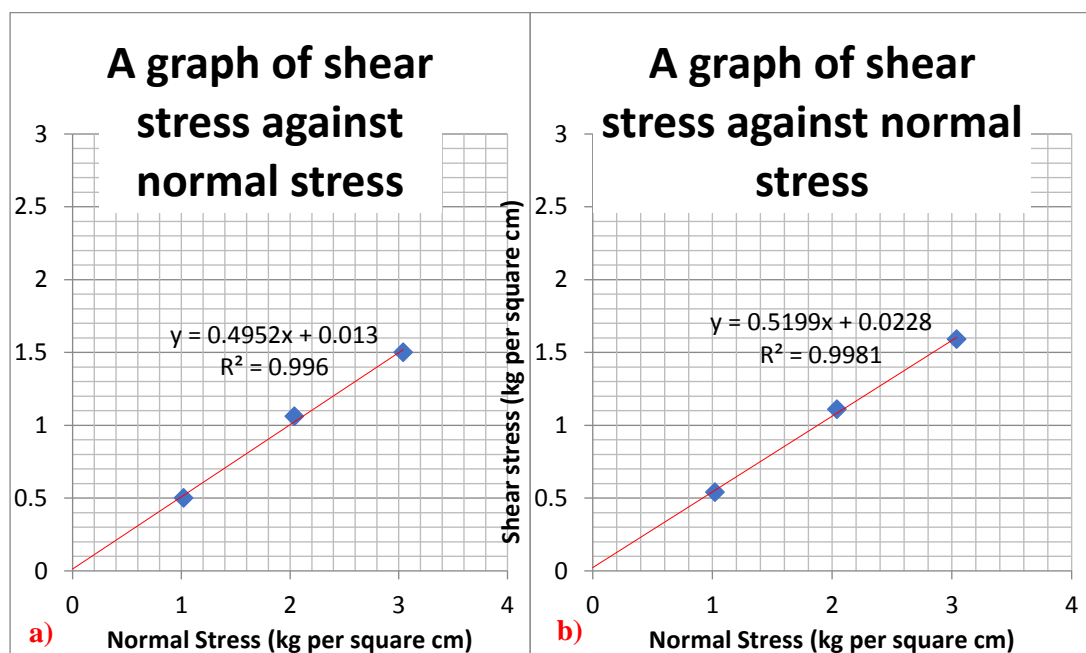
Figure 4.12 : Shear Test results for slope 1 (a) and slope 2 (b).

4.4.2.6 Uniaxial (unconfined) Compressive Strength

The test was carried out on both soils and rocks. Of course, in non-cohesive soils, this kind of test is limited but can provide supplementary information about shear strength. The unconfined compressive test is usually made on undisturbed samples. These are rock samples that were trimmed to different standardized dimensions. For the soil samples, the UCS values were smaller, ranging from 0.98 Kpa to 1,96 Kpa on the two slopes (Figure 4.12a and b). The results are presented in figure 4.14. For the rock samples, based on their weathering rate, the loading rate used was 0.5 % of the axial strain per minute. In general, the results revealed that the slope rocks have "poor strengths". The UCS (q_u) values are averaging between 41 Kpa for completely weathered black shale, 39 Kpa for moderately conglomerate, 64 and 54 Kpa for highly

weathered sandstone and pelite (Figure 4.13). The corresponding Undrained Shear Srengths S_u (Undrained cohesions CU) are given by the formula: $S_u=1/2q_u$, i.e 20.5 Kpa for strongly weathered blackshale, 19.5 Kpa for conglomerate, 32 Kpa for weathered sandstone and 27 Kpa for pelite.
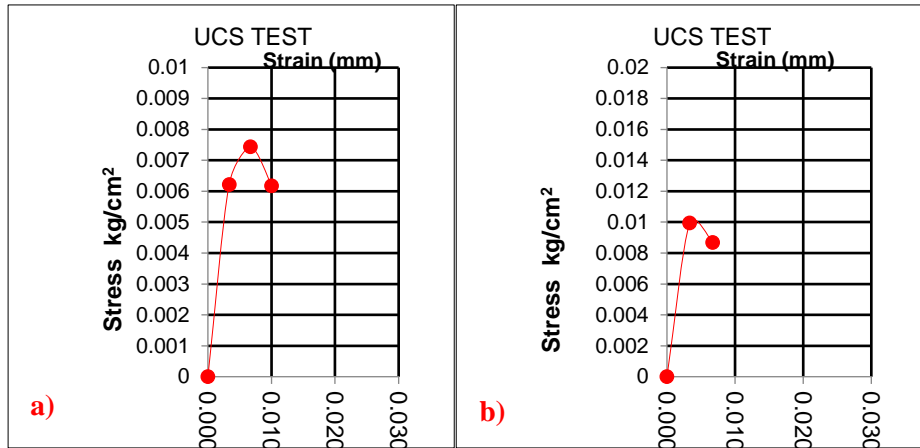
Figure 4.13: Typical curves of shear stress/strain from the UCS tests performed on soils for Slope 1(a) and slope2 (b).
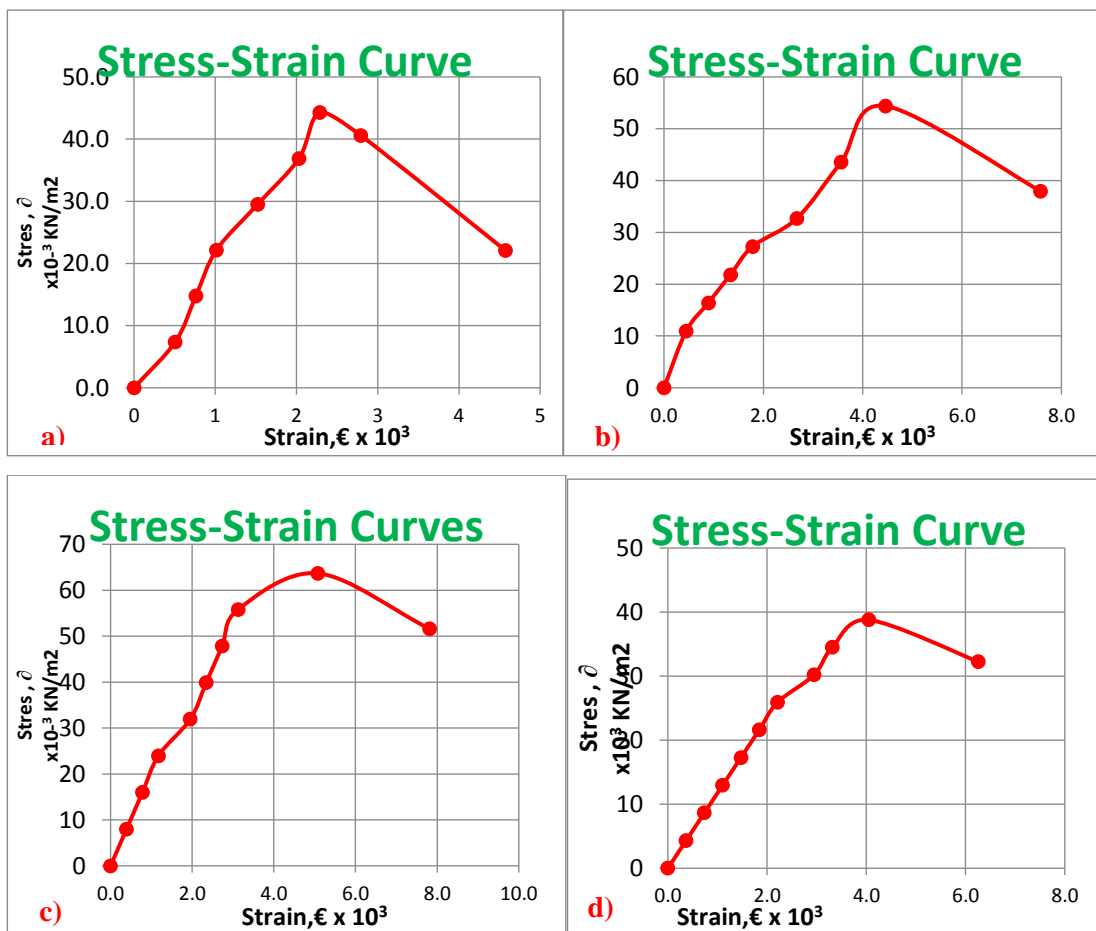
Figure 4.14 : Typical curves of shear stress/train from the UCS tests performed on C.W blackshale (a), H.W pelite (b) and sandstone (c), and M.W conglomerate (d).

The unconfined compressive strength and the Undrained Shear Strength values are smaller. This is justified not only by the weathering rate of the rocks but also by their mineralogical composition. The thin-section microscopy performed on black shale and pelitic rocks, both in plane polarized and crossed polarized lights, has revealed the presence of a significant amount of clay minerals (typically montmorillonites). The black color is attributed to the presence of carbon in the back shale and/or oxides in the pelite. Other minerals identified include quartz, feldspars, muscovite/sericite and chlorite (Figure 4.14). The presence of both oxides and montmorillonites in the rock matrix, makes these rocks potentially unsuitable for slope stability. This is due to the fact that, clay minerals tend to expand, when wetted, especially those of the montmorillonite group, and their increase in volume may create unexpected stress and strain in the ground. Furthermore, pyrite tends to oxidize on exposure, causing a decrease in rock strengths.
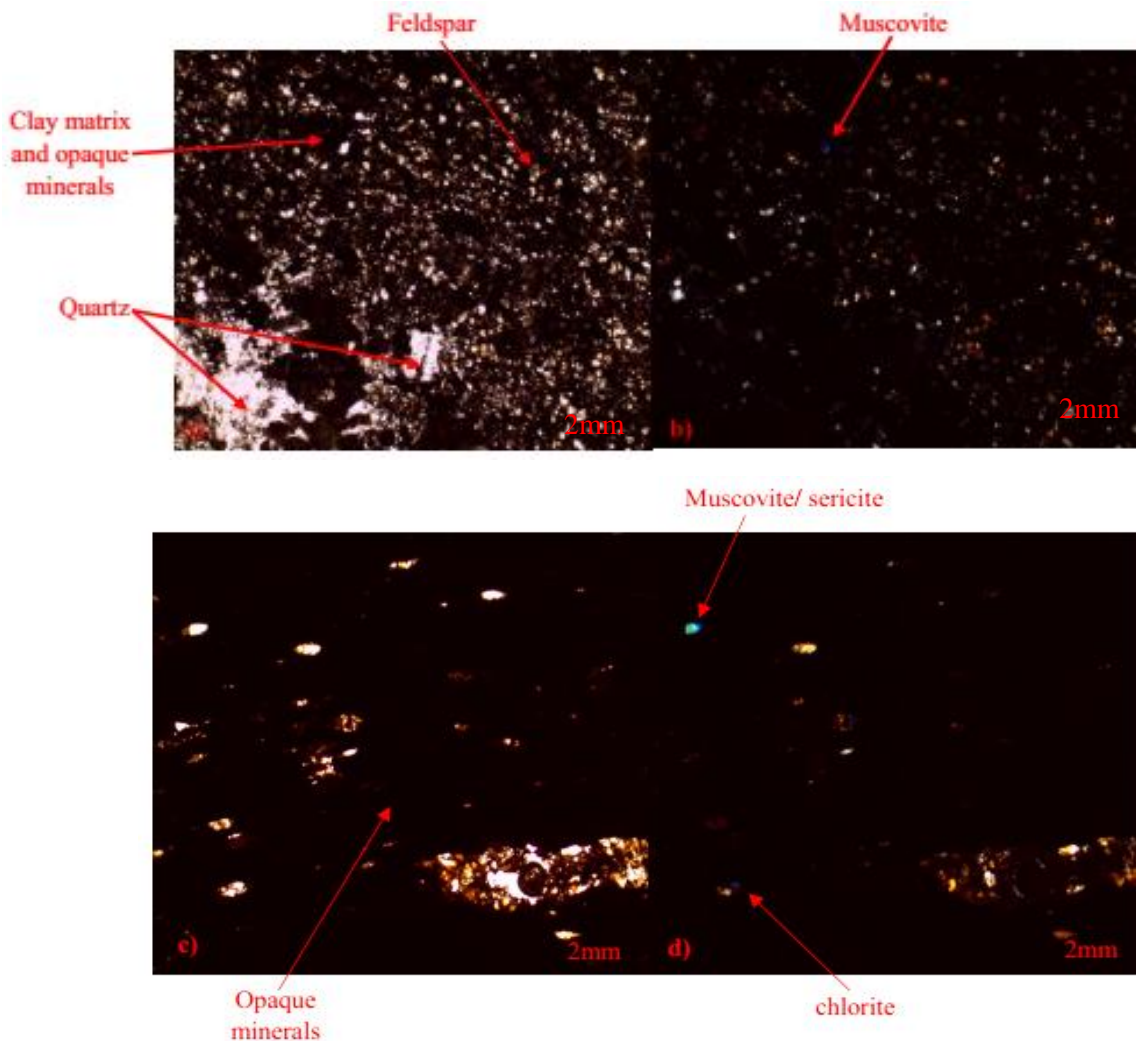
Figure 4.15 : Black shale and Pelite under microscope: Plane polarized light (a,c) and Cross polarized light (b,d).

4.5 DISCUSSION ON THE GEOTECHNICAL RESULTS AND COMPUTATION OF THE FACTOR OF SAFETY

The assessment of slope stability is also based on the expectation of a critical slip surface, and the computation of its factor of safety. The field investigations have revealed potential instabilities on the two slopes, with slip surfaces cutting through the entire slope profile. From the test results, we can see that R^2 values in strength tests are generally larger or equal to 0.99. This indicate the accuracy of the tests performed. Assessing material strength is one of the most critical factors in stability. The two methods utilized in this research have been efficiently used by different researchers in different soil and rock conditions. In addition, the methods have been used to directly and accurately acquire soil and rock strengths in zones of active movements where soil cohesions appear to become zero (Handy,1986).

4.5.1.1 Limit equilibrium

The procedure for assessing the factor of safety requires :

a. To develop the slope geometry and assign properties to the materials : The geometry was defined by the concept of regions. It is an intuitive approach aiming at drawing lines around the stratigraphic layers to form closed polygons. The heterogeneous slopes assessed are, respectively, 15 and 13m high. The sizes of the domain considered are 25 and 40 meters in width. The slope inclinations are : 38 degrees for slope (1) and 55 degrees for slope (2). The limit equilibrium method used in this analysis is the Morgenstern-Price Method.
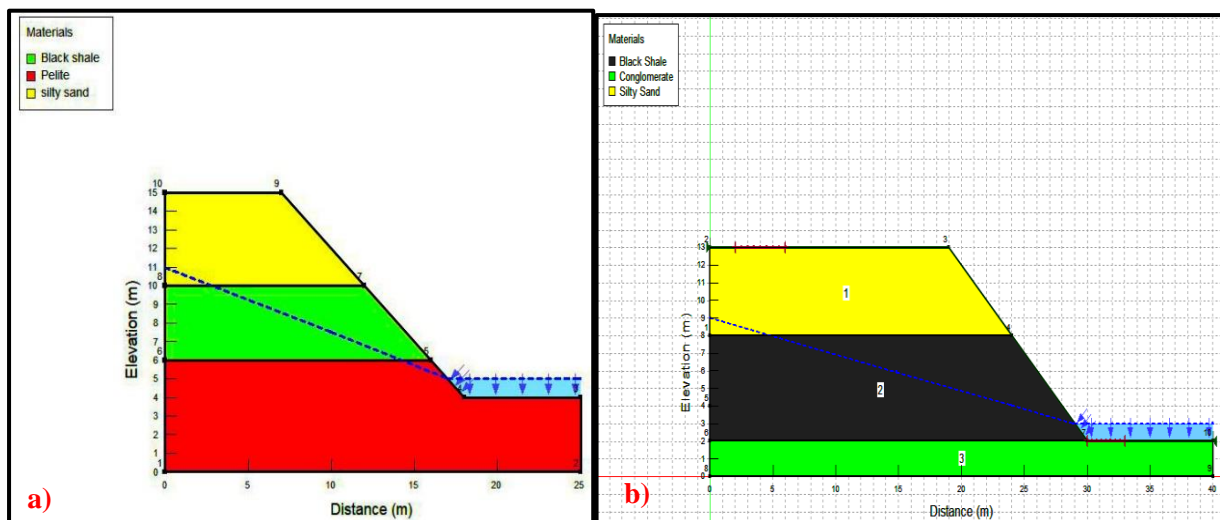
Figure 4.16 : Diagrams showing the slope regions and the corresponding materials. a) Slope 1, and b) slope 2

b. To define the failure surface and determine its geometry: In this assessment, the circular slip surfaces were considered given the fact that the failure happens in soils, underlaid by completely to highly weathered rocks with many intersecting weak planes / fractures. The sliding occurs along a curved surface forming a circular arc. The shear and the unconfined compressive tests have revealed that rocks and the soils have poor strengths. Hence, the critical slip surfaces occur at the interface between soils and black shales, but also cut through the underlying weak rocks.

The computation of the factor of safety has been done on the basis of the mechanical properties of soils and rocks. The pore water conditions were simulated in Slope/w program using a piezometric line i.e the pore waters were considered to be hydrostatic both below and above the piezometric line. The computed factors of safety were very small: $0.74 < FoS < 1$ for slope 1, and $0.48 < FoS < 1$ for slope 2 (Figure 16a and b).
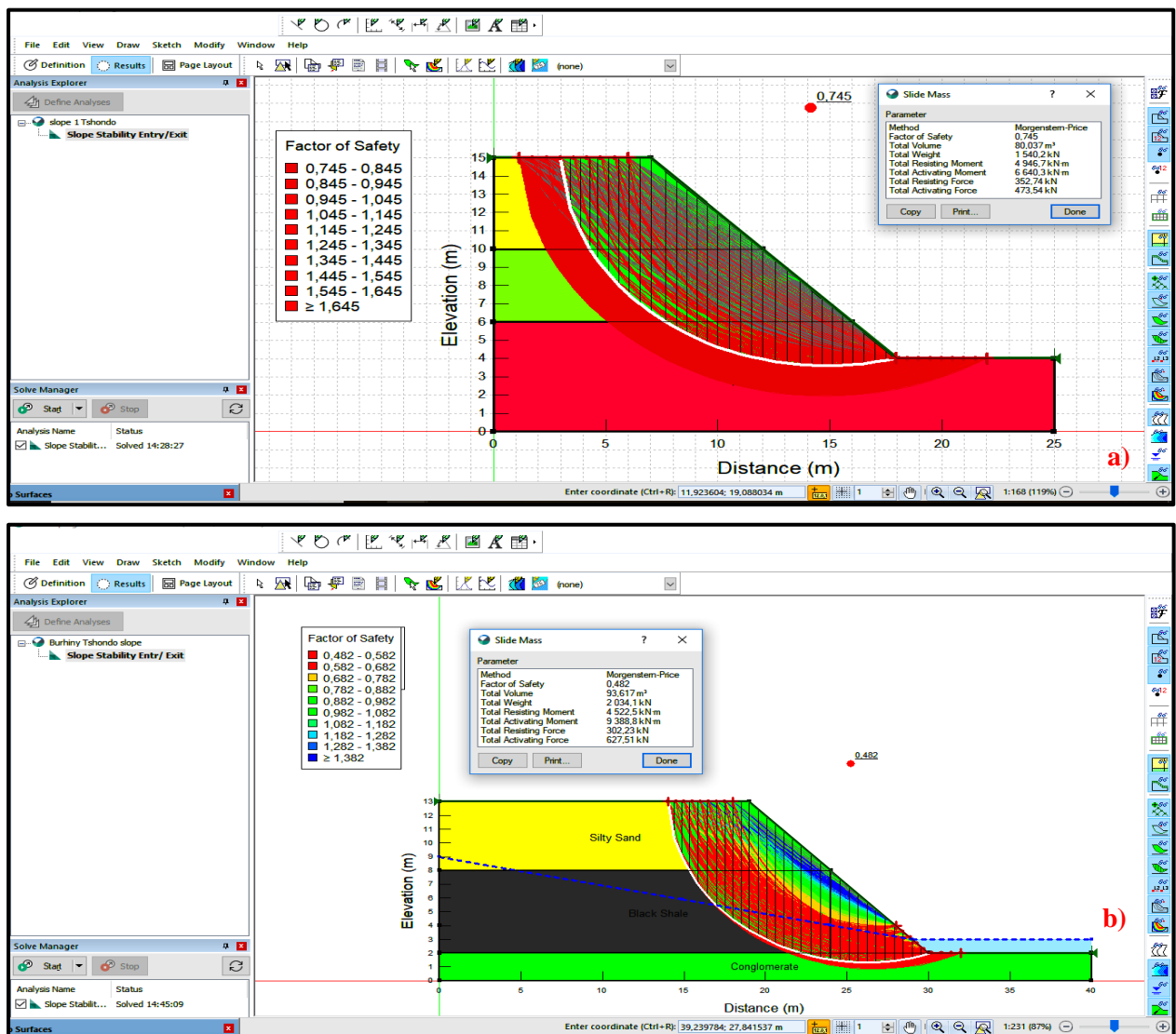
Figure 4.17: Factor of Safety for slope 1 (a) and slope 2(b).

54
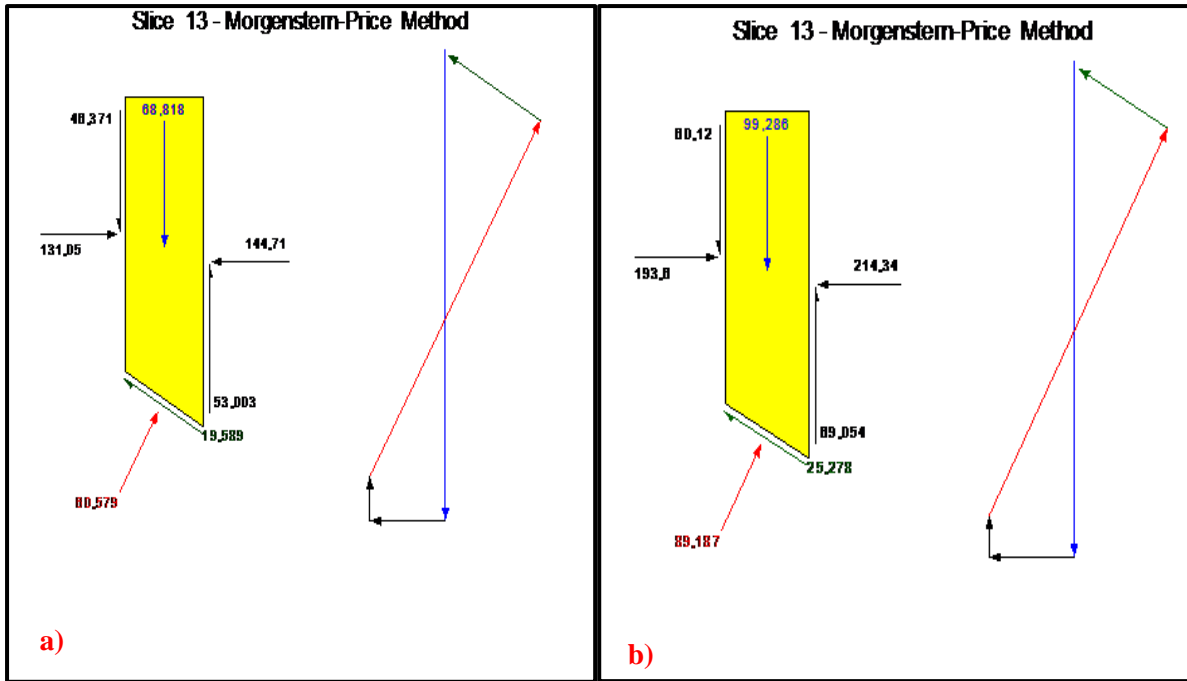
Figure 4.18: Slice free body diagrams and force polygons related to slope 1(a) and slope 2(b).

From these diagrams (Figure 4.18), it can be seen that all the forces acting on different slices are in equilibrium, since the polygon force closure is very good. This testifies the statement according to which the Morgensten-piece method satisfies both moment and force equilibriums.

4.5.1.2   Pseudostatic analysis

The coefficients used in practice mostly correspond to the acceleration values well below the predicted peak acceleration. The choice of the seismic coefficient was guided by the criteria recommended by Terzaghi (1950) who suggested this coefficient as ranging between 0.1 and 0.5. A coefficient of 0.1 describes severe earthquakes, 0.2 violent to destructive earthquakes and 0.5 catastrophic earthquakes. In the case of South-Kivu, after updating the earthquake catalog of the region for a period ranging from 1888 to 2015, Delvaux et Al (2016) performed a probabilistic seismic hazard assessment relying of the G-R (Gutenberg-Richter) parameters obtained from different seismic sources. They came up with 3 maps displaying different levels and patterns of peak ground accelerations. For the case of Tshondo, the average peak ground acceleration was 0.21g. This value corresponds to a K_h (seismic coefficient) of 0.21. After applying the seismic value into the analysis, the safety factors decreased significantly, by an amount equal to 1,34 times the values obtained in the previous case (Figure 4.19).
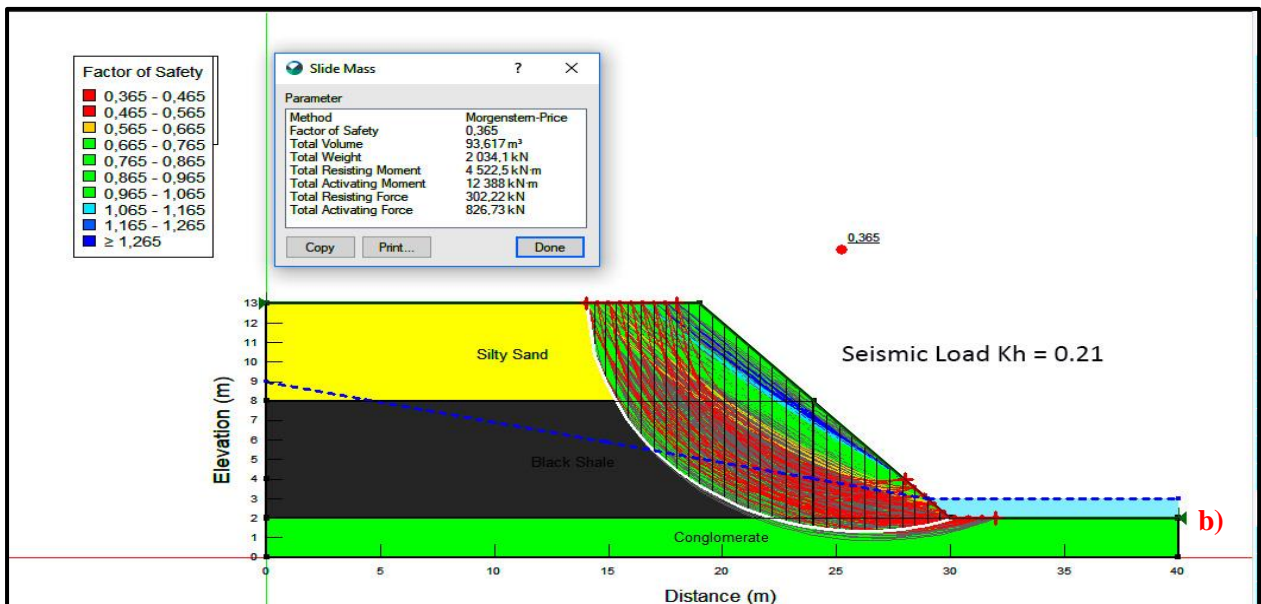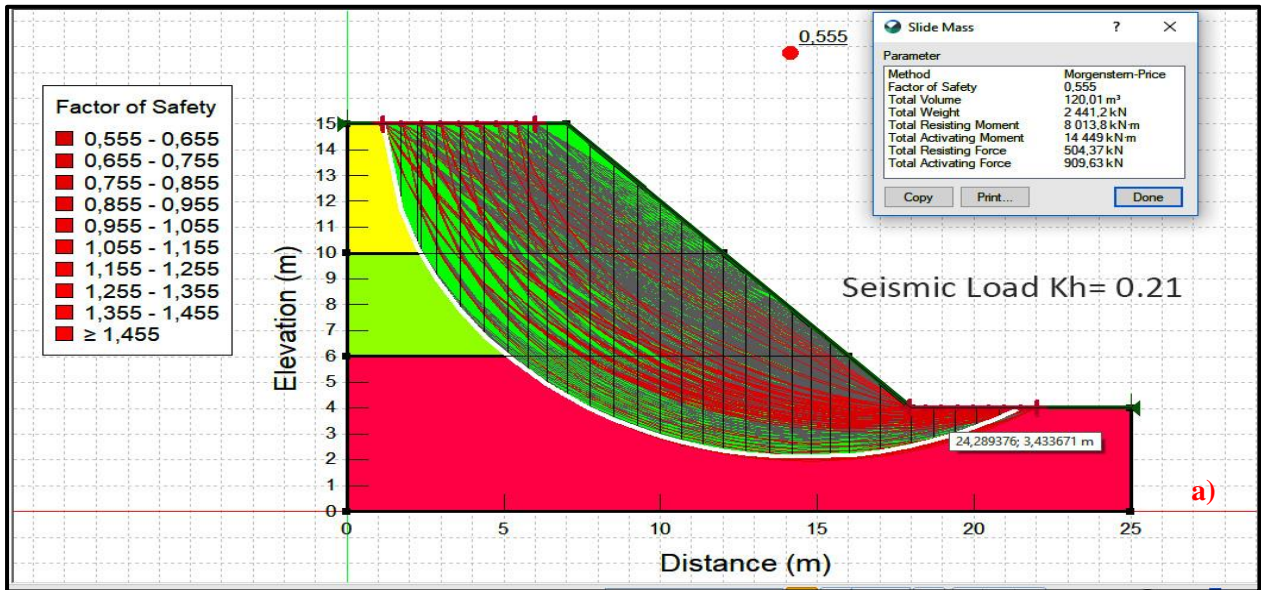
Figure 4.19: Factor of Safety for slope 1(a) and slope 2(b) under the effect of a seismic load.
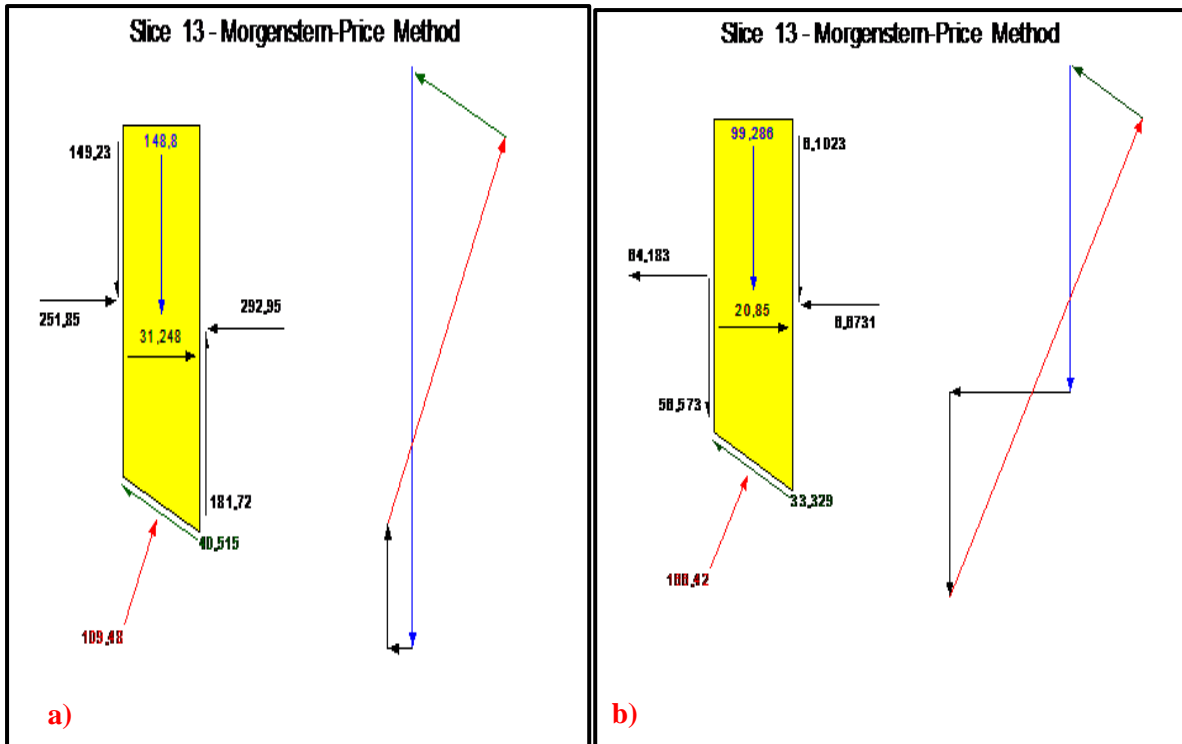
Figure 4.20: Free body diagrams and force polygons related to slope 1 & 2 in dynamic conditions.

Just like in the previous case, all the forces are in equilibrium, but here, the relative magnitudes of the driving forces increase significantly. The forces at the center of the slices represent the dynamic forces pointing in the sense of the movements (Figure 4.20).

CHAPTER 5 : CONCLUSION AND RECOMMENDATIONS

5.1   GENERAL INFORMATION

This thesis used both structural and geotechnical survey (supplemented with a thin section petrography) in order to determine whether the successive tectonic stresses to which Tshondo area has been subjected, together with the associated geological fractures as well as the fluctuation in soil and rock properties, are responsible for the recurrence of slope failures in the area. This chapter aims at providing the general conclusion and recommendations for further studies and for the risk management.

5.2   CONCLUSION

Slope stability analysis have been for longtime one of the subjects that many engineers have been focused on. Based on the objectives assigned to this research and the results obtained, we conclude that Tshondo lies within failure-prone terrains, where the instability of slopes is highly expected. This is aligned to the prevailing tectonic stresses affecting the area, the slip tendency values obtained for different fractures, and the safety factor values computed.

The structures generated by the submeridian tectonic were found to be generally trending NW-SE to N-S and ENE-WSW. From these orientations, from the principal stress axes given by $\sigma 1 \geq \sigma_2 \geq \sigma_3$ (N90º/65ºS, N186º/23ºNE, N250º/9ºSW), $\sigma_3 \geq \sigma_1 \geq \sigma_2$ (N44º/17ºSW, N133º/02º NW, N38º/73ºSW), and the stress ratio (0.46 and 2.5), It was ascertained that all the geological structures collected, originate from 2 phases of deformation. The compressional phase (D1-2) and the extensional phase (D2). The slip tendency values have revealed that slope failures are mostly triggered by sets of fault structures. Bedding surfaces, Joints, tensile and conjugate fractures on the other hand, are partially stable.

The geotechnical site and laboratory investigations, as well as the micro-petrography have established that both soils and rocks have poor strengths. This is partly due to the fact that the slopes highly weathered, but also, they are found in a highly strained zone, crossed by a series of faults considered to be tectonically active. The computation of the factor of safety was done using two limit equilibrium methods (Spencer and Morgenstern-price). The factors of safety for these two slopes were found to be less than 1 (0.74 and 0.48). By applying the peak ground acceleration to simulate dynamic conditions, it was noted that the factors of safety decreased significantly (0.55 and 0.36). This means that the uncompacted (loose) silty sand soils will tend

to liquefy under the effect of seismic loads. On the other hand, the underlying rocks will drastically lose their resisting strengths. If the groundwater table is disrupted in such a way that the hydrostatic equilibrium both below and above the piezometric surface(line) no longer exist, the water pressures will exceed the forces between the grains in the fractured rocks, causing their strengths to decrease further. Overall, in dry conditions the stability of slopes at Tshondo is compromised, but it gets more and more critical in drained and dynamic conditions.

5.3   RECOMMENDATIONS

5.3.1   Recommendations for further study

A monitoring system made of inclinometers and extensometers should be installed on various slopes at Tshondo to control the movement of fractures. Hot Spring temperatures should also be taken on a regular basis at Karhendezi/Kadubu in order to assess the extent of active deformations in the area. Piezometers should also be installed to control seasonal fluctuations in groundwater levels. The rainfall records should be gathered, as well as some ideas of the rate of infiltration and runoff.

The pore pressure should be assessed in order to verify the measurement of the effective stress. Geotechnical drilling (SPT tests) combined with Geophysical methods (Resistivity Tomography and Seismic Refraction) should be carried out in order to provide a complete information on the stratigraphy of slopes throughout the area.

5.3.2   Risk management

As mitigation measures, this study suggests the reprofiling of the slope geometry, and drainage by the introduction of shallowly inclined drainage holes. Support can also be used by placing weights at the foot of the slopes to resist downhill movements.

Artisanal operators need to become more aware of the danger to which their lives are exposed. A distinction must be made between strongly rugged and non-rugged reliefs. They should know that their activities (blasting, dewatering, removal of vegetation and water flow diversion), modify the physical agents of the environment in which they operate.

REFERENCES

Alén, C., 1998. On probability in geotechnics-Random calculation models exemplified on slope stability analysis and ground- superstructure interaction Department of Geotechnical Engineering. Chalmers University of Technology. 55-65pp.

Angelier, J., 1990. Inversion of field data in fault tectonics to obtain regional stress. III. A new rapid direct inversion method by analytical means. Geophysical Journal International 103, 363–376.

Angelier, J., 1994. Fault slip analysis and paleostress reconstruction. In : Hancock, P.L. (Ed.), Continental Deformation. Pergamon Press, Oxford, pp. 53–100.

Angelier, J., Tarantola, A., Manoussis, S., and Valette, B., 1982. Inversion of field data in fault tectonics to obtain the regional stress. Geophysical Journal of the Royal Astronomical Society 69, 607–621.

Aucelli, P., Casciello, E., Cesarano, M., Zampelli., S.P and Rosskopf, C.M., 2013. A deep, stratigraphically and structurally controlled landslide: the case of Mount La Civita (Molise, Italy). Landslides 10(5): 645–656.

Boven, A., Theunisseun, K., Sklyarov E., and Klerkx., J.,1999. Timing of exhumation of a high-pressure granulite terrane of the Paleoproterozoic Ubende belt (West Tanzania). Precambrian Research 93, 119-137.

Boutakoff., 1939. La Géologie des terrains situés à l'ouest et au Nord-Ouest du fossé tectonique du Kivu. Mém. Inst. Géol. Univ. Louvain, Belg., t.IX., 9, 17 – 207.

Bott, M. H., 1959. The mechanics of oblique slip faulting. Geol.Mag.96,19-11

Burg, J.P., Rumvegeri, B.T., Kampunzu, A.B., et Kapenda, D., 1987. Contraintes pétro-structurales dans l'évolution de la chaîne Kibarienne au Kivu (Zaïre).

Burrette, J., 1953. Les sols du Kivu. II, Carte des sols de la vallée de Kilombwe. Publ. CDKI, Bruxelles, Nouv. Sér.,

Byerlee, J., 1978. Friction of rocks. Pure and Applied Geophysics 116, 615–626. Caine, J., Evans, J., Forster, C., 1996. Fault zone architecture and permeability structure. Geology 24 (11), 1025–1028.

Cahen, L., 1954. The geology of Congo. Vaillant-Carmanne, Liège. 577pp.

Craig, T.J., Jackson, J.A., Priestley, K., and McKenzie, D.M., 2011. Earthquake distribution patterns in Africa: their relationship to variations in lithospheric and geological structures, and their rheological implications. Geophys. J. Int. 185, 403-434.

Cruden, D. M., 1991. A simple definition of a landslide. Bull. Eng. Geol. Environ., 43: 27-29.

Delvaux, D.,1993. The TENSOR program for paleostress reconstruction: example from the east African and the Baikal rift zones. Terra Nova 5(1): 216.

Delvaux, D, R Moeys, G Stapel, C Petit, K Levi, A Miroshnichenko, and V San'kov., 1997. Paleostress reconstructions and geodynamics of the Baikal region, Central Asia, Part 2. Cenozoic rifting. Tectonophysics 282(1–4): 1–38

Delvaux, D, and B Sperner., 2003. New aspects of tectonic stress inversion with reference to the TENSOR program. Geological Society, London, Special Publications 212(1): 75–100.

Delvaux, D., Jean-Luc, M., Mwene, N. S.S., Silvanos, F.B., François, K., and Hans-Balder, H., 2013. Seismic hazard assessment of the Kivu rift segment based on a new seismotectonic zonation in model. Journal of African Earth Sciences, 1-25pp, second edition.

Duncan, and James M., 1996. State of the art: limit equilibrium and finite-element analysis of slopes. Journal of Geotechnical engineering 122: 577-596.

Eduardo, Ga., Marta P., and Luigi P., 2013. weathering geochemistry and Sr-Nd fingerprints of equatorial upper Nile and Congo muds.Geochemistry, Geophysics and Geosystemes (G3).

Erick, K., Jean, B., Sebatien and L., Tubere, K., 2010. Developpement de la chefferie de Burhinyi. Observatoire Gouvernance et Paix (OGP). 66pp.

Espinoza, R., Repetto, P., and Muhunthan, B., 1992. General framework for stability analysis of slopes. Geotechnique 42: 603-615.

Fernandez-Alonso, M., Lavreau, J., and Klerkx, J., 1986. Geochemistry and geochronology of the Kibaran granites in Burundi, Central Africa: Implications for the Kibaran orogeny. – Chemical geology, 57, 217-234.

Ilunga, L., 1991. Morphologie, volcanisme et sédimentation dans le rift du Sud-Kivu, bulletin de la société géographique de liège, 27, 209-228.

Geiger, R., 1961. berarbeitete Neuausgabe von Geiger, R: Köppen-Geiger/Klima der Erde. Wandkarte (wall map) 1: 16 Mill. Klett-Perthes, Gotha.

Germain, R., Croegart J., and Sys C., 1955a. Carte des sols et de la végétation du Congo Belge et du Ruanda-Urundi. 3. Vallée de la Ruzizi, A. Sols (1 :1.000.000), B. Végétation (1:50.000). INEAC, Bruxelles.

Guiraud, M., O Laborde., and H Philip., 1989. Characterization of various types of deformation and their corresponding deviatoric stress tensors using microfault analysis. Tectonophysics 170(3–4) : 289–316.

Handy, R. L., 1986. Borehole shear test and slope stability. Proceedings of In-Situ '86. Geotechnical Division, ASCE. June 23-25, Blacksburg, VA. pp.161-175.

Hoek, E., and Bray, J. W., 1981, Rock Slope Engineering : The Institute of Mining and Metallurgy, London, England, 358 p.

Jaeger J.C., and Cook, N.G.W., 1969. Fundamentals of Rock Mechanics. Methuen, London.

Jaeger J.C., Cook NGW., and Zimmerman RW., 2007. Fundamentals of Rock Mechanics, 4th Edition. Blackwell, London.

Kampunzu, A.B., 1981, Le magmatisme du massif de Kahuzi (Kivu, Zaïre). Structure, pétrologie, signification et implication géodynamique. Thèse de doctorat.

Kanika, M.,1987. Contribution à la connaissance du volcanisme associé aux rifts intracontinentaux. Exemple des provinces volcaniques tertiaires, quaternaires de Mwenga Kamituga et de Bukavu dans le rift de l'Afrique Centrale (Sud - Bukavu, Zaïre). Succession des cycles volcaniques, nature et pétrogenèse des laves. Thèse doct. ès Sci. Univ. Lubumbashi, Fac. Sci. 219p.

Kanzira, H., 1989. Classification magmato-tectonique des granites du Rwanda. – IGCP n° 255 newsletter.

Kayen, JO., F Maerten., and DD Pollard., 2011. Mechanical analysis of fault slip data : implications for paleostress analysis. Journal of Structural Geology 33(2) : 78–91.

Lefévère, J., 2003. Analyse et interprétation de canevas lithostratigraphique et tectonique du Synclinal de l'Itombwe (Sud-Kivu République Démocratique du Congo) à l'aide des données satellitaires et radar.

Lepersonne, J., 1971. The basement formations in Maniema and Kivu-Mus. Roy.Afr. centr. Tervuren, Dépt. Géol. Min., Rapp. ann. 1970, 80-83.

Lhoest, A., 1946. Une coupe remarquable des couches de base de l'Urundi dans l'Itombwe (Congo beIge). Ann. Soc. Geol. Belg., 69, 250/258.

Lisle, R.J., and Srivastava, D.C., 2004. Test of the frictional reactivation theory for faults and validity of fault-slip analysis. Geology 32, 569–572.

Morris, A.P., Ferrill, D.A., and Henderson, D.B., 1996. Slip tendency and fault reactivation. Geology 24, 275–278.

Munyololo, Y., Wafula, M., Kasereka, M., Ciraba, M., Mukambilwa, K., Mavonga, T., Cirimwami, M., Muhigirwa, B., Bagalwa, R., and Mundala, M**.,** 1999. Récrudescence des glissements de terrain suite à la réactivation séismique du bassin du Lac Kivu. Région de Bukavu (Rép. Dém. Congo). Rapport Annuel du Département de Géologie et de Minéralogie du Musée Royal de l'Afrique Centrale 1997– 1998, 285–298.

Ogbonnaya,I., and Ikenna Anthony,O., 216. Application of paleostress analysis for the identification of potential instability precursors within the Benue Trough Nigeria, Department of Geology, Faculty of Physical Sciences, University of Nigeria, Nsukka, Nigeria.

Peeters, L., 1953. Tectonique du flanc oriental du synclinal de l'Itombwe Bull. Soc. Belge Géol., 61, 190/193.

Rumvegeri, B. T., 1984. Etudes lithostratigraphiques et structurales du précambrien de la région de Bunyakiri. Modèle d'évolution géodynamique de la chaîne Kibarienne en Afrique orientale et centrale. − Mém. D.E.S., Labor. Pétrologie, Univ. Lubumbashi, 183p.

Rumvegeri, B. T., 1987. Le Précambrien de l'Ouest du lac Kivu (Zaïre) et sa place dans l'évolution géodynamique de l'Afrique centrale et orientale. Pétrologie et Tectonique. Vol I.

Safiannikoff, A.,1950. Les systèmes de l'Urundi et de la Ruzizi au Kivu, et les intrusions granitiques. Annales de la Société géologique de Belgique. 73, 87–96p.

Sutton, G.H., Berg, and E.,1958. Seismological studies of the western Rift Valley of Africa. Trans. Am. Geophys. Union 39 (3), 474-481.

Terzaghi., 1950. Mechanism of Landslides. Geological society of America, Harvard University, Department of Engineering, 46p.

Turyomurugyendo, G., 1996. Some Aspects of Seismic Hazard in the East and South African Region. M.Sc. thesis. Institute of Solid Earth Physics, University of Bergen, Bergen, Norway, p. 80.

Villeneuve, M., 1976 a). Mise en evidence d'une discordance angulaire majeure dans les terrains precambriens au Nord du flanc oriental du "synclinal de l'Itombwe" (region du Kivu, Rep. du Zaire). C. R. Ao. Soi. Paris, 282, D, 1709/1712.

Villeneuve, M., 1977. Précambrien du Sud du lac Kivu. Etude stratigraphique, pétrographique et tectonique, Thèse Doct. Fac. Sci et Techn. St Jérôme, Marseille, France, 195 p.

Villeneuve, M., 1987. Géologie du synclinal de l'Itombwe (Zaïre oriental) et le problème de l'existence d'un sillon plisse Pan-africain, Jour nal of African Earth Sciences. 6 (6) 869-1l80.

Villeneuve, M., and Chorowicz, J., 2004. Les sillons plissés du Burundien supérieur dans la chaıne kibarienne d'Afrique centrale : Comptes Rendus Géoscience, v. 336, no. 9, p. 807-814.

Walemba, K.M.A., 2001. Geology, geochemistry, and tectono-metallogenic evolution of Neoproterozoic gold deposits in the Kadubu area, Kivu. Ph.D thesis, University of the Witwatersrand, Johannesburg, South Africa, 491 pp.+ Appendix 16 pp.

Walemba, K.M.A., and Master, S., 2005. Neoproterozoic diamictites from the Itombwe Synclinorium, Kivu Province, Democratic Republic of Congo: Palaeoclimatic significance and regional correlations: Journal of African Earth Sciences, v. 42, no. 1-5, p. 200-210.

Wilson, J.R. & Catsis, and M.C., 1990. A Preliminary survey of the forests of the 'Itombwe' Mountains and the KahuziBiega National Park Extension, East Zaire, July-Sept 1989. Unpublished report to WWF-FFPS-IZCN, Project 3902, Kinshasa.

Zana, N., Kavotha, K., and Wafula, M., 1992. Estimation of earthquake risk in Zaire. Tectonophysics 209, 321-323.

Zana, N., and Hamaguchi, H., 1978. Some characteristics of aftershock sequences in the western rift valley of Africa. Sci. Rep. Tohoku Univ. Ser. 5, Geophys. 25 (2), 55-72.

LIST OF APPENDICES

Appendix A 1: Table presenting the structural measurements of Tensile fractures and joints.

ID	Latitude Y (degre)	Longitude X (degre)	Elevation Z (m)	Dip (degree)	Dip directions(degree)	Strike (degree)	Observations	Lithology
1	-287,464	2,865,513	1340	85	76	166	Tensile fracture	Sandstone
2	-287,464	2,865,513	1340	79	42	132	Tensile fracture	Sandstone
3	-287,464	2,865,513	1340	80	54	144	Tensile fracture	Sandstone
4	-287,464	2,865,513	1340	75	43	133	Tensile fracture	Sandstone
5	-287,464	2,865,513	1340	75	34	124	Tensile fracture	Sandstone
6	-287,464	2,865,513	1340	76	40	130	Tensile fracture	Sandstone
7	-287,464	2,865,513	1340	76	34	124	Tensile fracture	Sandstone
8	-287,464	2,865,513	1340	70	42	132	Tensile fracture	Sandstone
9	-287,464	2,865,513	1340	71	43	133	Tensile fracture	Sandstone
10	-287,464	2,865,513	1340	75	40	130	Tensile fracture	Sandstone
11	-287,464	2,865,513	1340	75	44	134	Tensile fracture	Sandstone
12	-287,464	2,865,513	1340	76	45	135	Tensile fracture	Sandstone
13	-287,474	286,551	1344	89	52	142	Tensile fracture	Sandstone
14	-287,474	286,551	1344	87	55	145	Tensile fracture	Sandstone
15	-287,474	286,551	1344	82	40	130	Tensile fracture	Sandstone
16	-287,474	286,551	1344	87	60	150	Tensile fracture	Sandstone
17	-287,474	286,551	1344	85	42	132	Tensile fracture	Sandstone
18	-287,474	286,551	1344	85	45	135	Tensile fracture	Sandstone
19	-287,474	286,551	1344	71	42	132	Tensile fracture	Sandstone
20	-287,474	286,551	1344	70	44	134	Tensile fracture	Sandstone

21	-287,474	286,551	1344	88	34		124	Tensile fracture	Sandstone
22	-287,541	2,865,461	1340	85	32		122	Tensile fracture	Sandstone
23	-287,562	2,865,441	1355	74	35		125	Tensile fracture	Sandstone
24	-287,562	2,865,441	1355	71	32		122	Tensile fracture	Sandstone
25	-287,562	2,865,441	1355	85	44		134	Tensile fracture	Sandstone
26	-287,562	2,865,441	1355	75	52		142	Tensile fracture	Sandstone
27	-287,562	2,865,441	1355	52	32		122	Tensile fracture	Black Shale
28	-287,562	2,865,441	1355	67	54		144	Tensile fracture	Black Shale
29	-287,491	2,865,592	1348	66	50		140	Tensile fracture	Black Shale
30	-287,491	2,865,592	1348	45	44		134	Tensile fracture	Black Shale
31	-287,515	2,865,637	1345	70	60		150	Tensile fracture	Black Shale
32	-287,515	2,865,637	1356	49	22		112	Tensile fracture	Black Shale
33	-287,515	2,865,637	1351	53	34		124	Tensile fracture	Black Shale
34	-287,515	2,865,637	1351	65	52		142	Tensile fracture	Black Shale
35	-287,515	2,865,637	1353	61	55		145	Tensile fracture	Black Shale
36	-287,731	2,865,761	1454	39	32		122	Tensile fracture	Black Shale
37	-287,731	2,865,761	1448	75	63		153	Tensile fracture	Black Shale
38	-287,731	2,865,761	1454	45	42		132	Tensile fracture	Black Shale
39	-287,731	2,865,761	1447	45	52		142	Tensile fracture	Black Shale
40	-287,731	2,865,761	1454	41	44		134	Tensile fracture	Black Shale
41	-287,688	2,865,811	1454	40	41		131	Tensile fracture	Black Shale

42	-287,688	2,865,811	1454	39	32	122	Tensile fracture	Black Shale
43	-287,688	2,865,811	1446	42	24	114	Tensile fracture	Black Shale
44	-287,688	2,865,811	1446	44	58	148	Tensile fracture	Black Shale
45	-287,818	2,865,897	1439	44	43	133	Tensile fracture	Black Shale
46	-287,818	2,865,897	1439	53	30	120	Tensile fracture	Black Shale
47	-287,691	2,865,874	1456	37	16	106	Tensile fracture	Black Shale
48	-287,691	2,865,874	1456	44	44	134	Tensile fracture	Black Shale
49	-287,691	2,865,874	1456	40	42	132	Tensile fracture	Black Shale
50	-287,691	2,865,874	1456	42	45	135	Tensile fracture	Black Shale
51	-287,691	2,865,874	1456	35	32	122	Tensile fracture	Black Shale
52	-287,691	2,865,874	1456	39	34	124	Tensile fracture	Black Shale
53	-287,691	2,865,874	1456	39	30	120	Tensile fracture	Black Shale
54	-287,691	2,865,874	1456	64	69	159	Tensile fracture	Black Shale
55	-287,691	2,865,874	1456	65	69	159	Tensile fracture	Black Shale
56	-285,733	2,865,827	1445	49	26	116	Tensile fracture	Black Shale
57	-285,733	2,865,827	1445	50	28	118	Tensile fracture	Black Shale
58	-285,733	2,865,827	1445	41	22	112	Tensile fracture	Black Shale
59	-285,733	2,865,827	1445	38	10	100	Tensile fracture	Black Shale
60	-285,733	2,865,827	1345	44	140	230	Tensile fracture	Black Shale
61	-287,568	2,865,882	1340	85	52	142	Tensile fracture	Black Shale

62	-287,568	2,865,882	1346	72	42		132	Tensile fracture	Black Shale
63	-287,584	2,865,888	1343	60	35		125	Tensile fracture	Black Shale
64	-287,584	2,865,888	1363	59	20		110	Tensile fracture	Black Shale
65	-287,584	2,865,888	1363	70	38		128	Tensile fracture	Black Shale
66	-28,741	2,865,462	1319	64	44		134	Tensile fracture	Black Shale
67	-28,741	2,865,462	1319	61	18		108	Tensile fracture	Black Shale
68	-287,397	2,865,886	1318	54	38		128	Tensile fracture	Black Shale
69	-287,458	2,865,505	1315	68	35		125	Tensile fracture	Black Shale
70	-28,746	2,865,511	1314	70	28		118	Tensile fracture	Black Shale
71	-285,509	28,656	1352	66	48		138	Tensile fracture	Black Shale
72	-285,509	28,656	1352	67	52		142	Tensile fracture	Black Shale
73	-287,542	2,867,637	1381	49	28		118	Tensile fracture	Black Shale
74	-287,542	2,867,637	1381	53	32		122	Tensile fracture	Black Shale
75	-287,841	2,865,871	1456	40	56		146	Joint	Black Shale
76	-287,904	286,527	1456	60	82		172	Joint	Black Shale
77	-287,812	28,659	1454	55	50		140	Joint	Black Shale
78	-287,812	28,659	1456	60	64		154	Joint	Black Shale
79	-287,549	2,865,672	1342	46	36		126	Joint	Black Shale
80	-287,549	2,865,672	1342	46	14		104	Joint	Black Shale
81	-287,472	2,865,511	1348	81	40		130	Joint	Black Shale
82	-287,476	2,865,503	1317	75	30		120	Joint	Black Shale
83	-287,435	2,865,801	1373	70	50		140	Joint	Black Shale
84	-287,167	286,783	1398	57	10		100	Joint	Black Shale
85	-287,167	286,783	1398	56	10		100	Joint	Black Shale

86	-287,167	286,783	1398	50	70		160	Joint	Black Shale
87	-287,546	2,865,895	1330	72	23		113	Joint	Black Shale
88	-287,564	2,865,927	1346	65	34		124	Joint	Black Shale
89	-287,482	2,865,847	1336	59	45		135	Joint	Black Shale
90	-2.87443	28.65554	1331	45	10		100	Joint	Black shale
91	-2.87208	28.6729	1449	79	53		143	Joint	Black shale
92	-2.87208	28.6729	1449	70	51		141	Joint	Black shale
93	-2.87208	28.6729	1449	80	68		158	Joint	Black shale
94	-2.87208	28.6729	1449	70	78		168	Joint	Black shale
95	-2.87585	28.65409	1358	74	110		200	Joint	Black shale
96	-2.8762	28.6766	1440	66	91		181	Joint	Black shale
97	-2.87701	28.65816	1444	86	336		66	Joint	Black shale
98	-2.87868	28.66009	1492	88	352		82	Joint	Black shale
99	-2.87496	28.65596	1349	65	263		353	Joint	Black shale
100	-2.87196	28.673	1416	49	37		127	Joint	Black shale
101	-2.87516	28.65844	1325	20	99		189	Joint	Black shale
102	-2.87688	28.65811	1446	85	142		232	Joint	Black shale
103	-2.87691	28.65874	1356	75	52		142	Joint	Black shale
104	-2.87691	28.65874	1356	85	340		70	Joint	Black shale
105	-2.87691	28.65874	1356	69	162		252	Joint	Black shale
106	-2.87691	28.65874	1356	64	156		246	Joint	Black shale

Appendix A 2: Data from the density determination test.

University of Nairobi

Department of Civil & Construction Engineering

(Soil Mechanics Laboratory)

BULK DENSITY

CLIENT	AGANZE/Msc Student					
PROJECT	TSHONDO					
Depth (m)	3m	Test pit ID:	U100	Sample Type	UNDISTURBED SAMPLE	
Test date:	27-Apr-18	Sample Description:	silty sands			
Specification	According to BS 1377:1990			Location:	TSHONDO/DR.Congo	

Sample Number		SLOPE 1	SLOPE 2	
Mass of core cutter + Wet soil(g)		3410	4974	
Mass of core cutter(g)		2000	2050	
Mass of wet soil(g)		1410	2924	
Volume of core cutter(cm3)		1997	2012	
Bulk density (g/cm3)		0.706	1.453	
Container No.		120	51	
Mass of wet soil + Container(g)		250	224	
Mass of dry soil + Container(g)		221	219	
Mass of Container(g)		113.8	95	
Loss in Moisture (g)		29	5	
Mass of Dry soil		107.2	124	
Moisture Content (%)		27.1	4.0	
Dry density(g/cm3)		0.556	1.397	

70

Appendix A 3: Data from the specific gravity determination test.

University of Nairobi

Department of Civil & Construction Engineering

(Soil Mechanics Laboratory)

SPECIFIC GRAVITY

CLIENT	AGANZE/ MSc. Student					
PROJECT	TSHONDO					
Depth (m)	3m	Test pit ID:		Sample. No.	slope 1&2	
Test date:	02-May-18	Sample Description:	clayey silt			
Specification	According to BS 1377:1990 Part			Location:	TSHONDO/DRC	

					SLOPE 1	SLOPE 2		
Sample Number								
Bottle Number					2	3		
Mass of empty bottle (W_1)					70	66		
Mass of bottle + Soil (W_2)					79.7	76.1		
Mass of bottle + Soil+ Water (W_3)					190	186.4		
Mass of bottle full of Water (W_4)					184.1	180.2		
Mass of Water used (W_{3-W2})					110.3	110.3		
Mass of soil used (W_{2-W1})					9.7	10.1		
Volume of Soil (W_4-W_1)-(W_3-W_2)					3.8	3.9		
Specific Gravity of Soil $$GS = \frac{(W2-W1)}{(W4-W1)-(W3-W2)}$$					2.553	2.590		

71

Appendix A 4: Data from the sieve and hydrometer Analyses.

SIEVE ANALYSA5:X36IS

CLIENT	AGANZE/MSc Student											
PROJECT	TSHONDO/ DR.Congo											
Depth (m)	3m			SAMPLE No		SLOPE 1						
Test date:	02-May-18			Specimen			silty sand					
Specification	According to BS 1377:1990											

Pan mass	(gm)	0				
Initial dry sample mass + pan	(gm)					
Initial dry sample mass	(gm)	200	Fine mass			55.6
Washed dry sample mass + pan	(gm)		Fine percent			27.8
Washed dry sample mass	(gm)	144.4	Acceptance Criteria			

Wet & Dry Sieve Analysis to BS 1377				Hydrometer Analysis to BS 1377								
Sieve size (mm)	Retained mass (gm)	% Retained (%)	Cumulative passed percentage (%)	Date	Time In min	Temp ^{o} C.	Rh1	Rh	HR	D(mm)	K(%)	K(corrected)
20	0	0.0	100.0	9AM	0.5	20	28.0	28.5	8.9	0.05713	89	25
10	35.7	17.9	82.2									
5	26.1	13.1	69.1									
2.36	21.2	10.6	58.5		1	20	23.5	24	9.6	0.04195	75	21
1.18	15.9	8.0	50.6		2	20	18.5	19	11	0.03175	58	16
0.6	11.3	5.7	44.9		4	20	13.5	14	14.8	0.02604	42	12
0.425	7.1	3.6	41.4		8	20	8.5	9	16.3	0.01933	26	7
0.3	7.4	3.7	37.7		15	20	5.5	6	13.9	0.01303	16	5
0.15	9.9	5.0	32.7		30	20	4.5	5	18.3	0.01058	13	4
0.075	9.8	4.9	27.8		60	20	4.5	5	18.3	0.00748	13	4
<0.075	55.6	27.8			240	20	4.5	5	18.3	0.00374	13	4
TOTAL	200				480	20	4.5	5	18.3	0.00264	13	4
					1440	20	4.5	5	18.3	0.00153	13	4

University of Nairobi

Department of Civil & Construction Engineering
(Soil Mechanics Laboratory)

SIEVE ANALYSIS

C+A8:X40LIENT	AGANZE /MSc.Student			
PROJECT	TSHONDO/DR.Congo			
Depth (m)	3m	SAMPLE No	SLOPE 2	
Test date:	02-May-18	Specimen		silty sand
Specification	According to BS 1377:1990			

Pan mass	(gm)			
Initial dry sample mass + pan	(gm)			
Initial dry sample mass	(gm)	100	Fine mass	16.3
Washed dry sample mass + pan	(gm)		Fine percent	16.3
Washed dry sample mass	(gm)	83.7	Acceptance Criteria	

Wet & Dry Sieve Analysis to BS 1377				Hydrometer Analysis to BS 1377									
Sieve size (mm)	Retained mass (gm)	% Retained (%)	Cumulative passed percentage (%)	Date	Time In min	Temp ° C.	Rh1	Rh	HR	D(mm)	K(%)	K(corrected)
20	0	0.0	100.0	9AM	0.5	20	29.0	29.5	8.6	0.05615	92	15
10	9.5	9.5	90.5									
5	11.7	11.7	78.8									
2.36	9.6	9.6	69.2		1	20	25.0	25.5	10.2	0.04324	79	13
1.18	8	8.0	61.2		2	20	22.0	22.5	11.4	0.03233	70	11
0.6	7.7	7.7	53.5		4	20	18.5	19	12.7	0.02413	58	10
0.425	6.7	6.7	46.8		8	20	13.5	14	14.7	0.01835	42	7
0.3	7.3	7.3	39.5		15	20	11	11.5	15.7	0.01385	34	6
0.15	12.5	12.5	27.0		30	20	8.5	9	16.7	0.0101	26	4
0.075	10.7	10.7	16.3		60	20	6	6.5	17.6	0.00733	18	3
<0.075	16.3	16.3			240	20	5	5.5	18	0.00371	15	2
TOTAL	100				480	20	4.5	5	18.3	0.00264	13	2
					1440	20	4.5	5	18.3	0.00153	13	2

73

Appendix A 5: Data from the direct shear test.

University of Nairobi
Department of Civil & Construction Engineering
(Soil Mechanics Laboratory)

CLIENT : AGANZE /Msc. Student
SITE: TSHONDO/DRC

| **DEPTH : 3m** | | | **S/no : SLOPE 1** |

SPECIFICATION : According to BS 1377:

DIRECT SHEAR TEST

LOADS APPLIED

weight of hanger = 4.5 kg			**Area of shear box =** 36 square cm
1st load = 32.2 kg			
Total = 1st load + weight of hanger =	36.7	kg	

| **2nd load   =68.9 kg** | | | |
| Total   = 2nd load + weight of hanger = | 73.4 | kg | |

| **3rd load   = 105kg** | | | |
| Total   = 3rd load + weight of hanger = | 109.5 | kg | |

Normal stress = applied load/area of shear box   **shear stress = shear force at failure/ area of shear box**

Normal stress =	1.02	kg per square cm	Shear stress =	0.5	kg per square cm
Normal stress =	2.04	kg per square cm	Shear stress =	1.06	kg per square cm
Normal stress =	3.04	kg per square cm	Shear stress =	1.5	kg per square cm

University of Nairobi
Department of Civil & Construction Engineering
(Soil Mechanics Laboratory)

CLIENT : AGANZE /Msc. Student
SITE: TSHONDO/DR.Congo

DEPTH : 3m		S/no : SLOPE2	

SPECIFICATION : According to BS 1377:1990

DIRECT SHEAR TEST

LOADS APPLIED

weight of hanger = 4.5 kg   **Area of shear box = 36 square cm**

1st load = 32.2 kg			
Total = 1st load + weight of hanger =	36.7	kg	

2nd load =68.9 kg			
Total = 2nd load + weight of hanger =	73.4	kg	

3rd load = 105kg			
Total = 3rd load + weight of hanger =	109.5	kg	

Normal stress = applied load/area of shear box   **shear stress = shear force at failure/ area of shear box**

Normal stress =	1.02	kg per square cm	Shear stress =	0.54	kg per square cm	
Normal stress =	2.04	kg per square cm	Shear stress =	1.11	kg per square cm	
Normal stress =	3.04	kg per square cm	Shear stress =	1.59	kg per square cm	

Appendix A 6: Data from the Unconfined Compressive Strengths (UCS)/Soil samples.

A1:Q20B7A1 UNIVERSITY OF NAIROBI

(SOIL MECHANICS LABORATORY)

WORKING SHEET

UCS TEST

(BS 1377/BS1924:1990)

CLIENT: AGANZE/Msc.Student		PROVING RING NO.	4980
SAMPLE. SLOPE 1		CALIBRATION FACTOR	0.141Kg/Div

DATA		SAMPLE DETAILS		
Do =cm	3.8	Type	NEAT	
Lo (cm)	7.6	Stabilizer	N/A	
Ao =(3.142x3.8x3.8)/4 cm²	11.3	%		
Volume = AoLo cm³	86	Type		

Defl.	Deflection			Stress	
	E=L/L0	1-E	A=(Ao)/1-E	Load	Q
mm				Kg	Kg/cm²
0	0	1	11.30000	0	0
0.254	0.0033	0.99666	11.33789	0.1	0.006
0.508	0.0067	0.99332	11.37604	0.1	0.007
0.762	0.0100	0.98997	11.41444	0.0705	0.006

UNIVERSITY OF NAIROBI

(SOIL MECHANICS LABORATORY)

WORKING SHEET

UCS TEST

(BS 1377/BS1924:1990)

CLIENT: AGANZE/Msc.Student		PROVING RING NO.	4980
SAMPLE. SLOPE 2		CALIBRATION FACTOR	0.141Kg/Div

DATA		SAMPLE DETAILS		
Do =cm	3.8	Type	NEAT	
Lo (cm)	7.6	Stabilizer	N/A	
Ao =(3.142x3.8x3.8)/4 cm²	11.3	%		
Volume = AoLo cm³	86	Type		

Defl.	Deflection			Stress	
	E=L/L0	1-E	A=(Ao)/1-E	Load	Q
mm				Kg	Kg/cm²
0	0	1	11.30000	0	0
0.254	0.0033	0.99666	11.33789	0.1	0.010
0.508	0.0067	0.99332	11.37604	0.1	0.009

Appendix A 7: Data from the Unconfined Compressive Strengths (UCS)/Rock samples.

BLACKSHALE

Length (mm)	52	UCS (KN/m²)	41		
Width (mm)	52				
Height (mm)	54	Density (Kg/m³)	2382		
Mean Area (mm²)	2704	Water Absorption	8%		
Volume (mm³)	146016	**Unit weight (Kg/m³)**	2675		

Deformation Gauge Reading	Compression of Specimen ΔL (mm)	Strain $\epsilon = \Delta L/Lo$	Axial force P (KN)	Corrected Area $A = Ao/(1 - \epsilon)$ mm^2	Corrected Axial Stress $\sigma_1 = P/A$ (kN/m^2)
0	0.00	0.0000	0.0000	2704	0
1	0.03	0.0005	0.0200	2705	7
1.5	0.04	0.0008	0.0400	2706	15
2	0.05	0.0010	0.0600	2707	22
3	0.08	0.0015	0.0800	2708	30
4	0.10	0.0020	0.1000	2710	37
4.5	0.11	0.0023	0.1200	2710	44
5.5	0.14	0.0028	0.1100	2712	41
9	0.23	0.0046	0.0600	2716	22

CONGLOMERATE

Length (mm)	68	UCS (KN/m²)	39		
Width (mm)	68				
Height (mm)	69	Density (Kg/m³)	2504		
Mean Area (mm²)	4624	Water Absorption	3%		
Volume (mm³)	319056	**Unit weight (Kg/m³)**	2633		

Deformation Gauge Reading	Compression of Specimen ΔL (mm)	Strain $\epsilon = \Delta L/Lo$	Axial force P (KN)	Corrected Area $A = Ao/(1 - \epsilon)$ mm^2	Corrected Axial Stress $\sigma_1 = P/A$ (kN/m^2)
0	0.00	0.0000	0.00	4624	0
1	0.03	0.0004	0.02	4626	4
2	0.05	0.0007	0.04	4627	9
3	0.08	0.0011	0.06	4629	13
4	0.10	0.0015	0.08	4631	17
5	0.13	0.0018	0.10	4633	22
6	0.15	0.0022	0.12	4634	26
8	0.20	0.0029	0.14	4638	30
9	0.23	0.0033	0.16	4639	34
11	0.28	0.0040	0.18	4643	39
17	0.43	0.0063	0.15	4653	32

PELITE

Length (mm)	50	UCS (KN/m²)	54		
Width (mm)	50				
Height (mm)	57	Density (Kg/m³)	2473		
Mean Area (mm²)	2500	Water Absorption	8%		
Volume (mm³)	142500	**Unit weight (Kg/r**	2818		

Deformation Gauge Reading	Compression of Specimen ΔL (mm)	Strain $\epsilon = \Delta L / Lo$	Axial force P (KN)	Corrected Area $A = Ao/(1 - \epsilon)$ mm^2	Corrected Axial Stress $\sigma_1 = P/A$ (kN/m^2)
0	0.00	0.0000	0.00	2500	0
1	0.03	0.0004	0.04	3662	11
2	0.05	0.0009	0.06	3663	16
3	0.08	0.0013	0.08	3665	22
4	0.10	0.0018	0.10	3667	27
6	0.15	0.0027	0.12	3670	33
8	0.20	0.0036	0.16	3673	44
10	0.25	0.0045	0.20	3676	54
17	0.43	0.0076	0.14	3688	38

SANDSTONE

Length (mm)	50	UCS (KN/m²)	64		
Width (mm)	50				
Height (mm)	65	Density (Kg/m³)	2557		
Mean Area (m	2500	Water Absorption	3%		
Volume (mm³)	162500	**Unit weight (Kg/r**	2666		

Deformation Gauge Reading	Compression of Specimen ΔL (mm)	Strain $\epsilon = \Delta L / Lo$	Axial force P (KN)	Corrected Area $A = Ao/(1 - \epsilon)$ mm^2	Corrected Axial Stress $\sigma_1 = P/A$ (kN/m^2)
0	0.00	0.0000	0.00	2500	0
1	0.03	0.0004	0.02	2501	8
2	0.05	0.0008	0.04	2502	16
3	0.08	0.0012	0.06	2503	24
5	0.13	0.0020	0.08	2505	32
6	0.15	0.0023	0.10	2506	40
7	0.18	0.0027	0.12	2507	48
8	0.20	0.0031	0.14	2508	56
13	0.33	0.0051	0.16	2513	64
20	0.51	0.0078	0.13	2520	52